SANDIA REPORT
SAND2015-8394
Unlimited Release
Printed September 2015

Uniaxial Creep as a Control on Mercury Intrusion Capillary Pressure in Consolidating Rock Salt

Thomas Dewers, Jason Heath
Geomechanics Department

And

Christi Leigh
Repository Performance Department
Sandia National Laboratories

Prepared by
Sandia National Laboratories
Albuquerque, New Mexico 87185 and Livermore, California 94550

Sandia National Laboratories is a multi-program laboratory managed and operated by Sandia Corporation, a wholly owned subsidiary of Lockheed Martin Corporation, for the U.S. Department of Energy's National Nuclear Security Administration under contract DE-AC04-94AL85000.

Issued by Sandia National Laboratories, operated for the United States Department of Energy by Sandia Corporation.

Available to DOE and DOE contractors from
U.S. Department of Energy
Office of Scientific and Technical Information
P.O. Box 62
Oak Ridge, TN 37831

Telephone: (865) 576-8401
Facsimile: (865) 576-5728
E-Mail: reports@adonis.osti.gov
Online ordering: http://www.osti.gov/bridge

Available to the public from
U.S. Department of Commerce
National Technical Information Service
5285 Port Royal Rd.
Springfield, VA 22161

Telephone: (800) 553-6847
Facsimile: (703) 605-6900
E-Mail: orders@ntis.fedworld.gov
Online order: http://www.ntis.gov/help/ordermethods.asp?loc=7-4-0#online

SAND2015-8394
Unlimited Release
Printed September 2015

Uniaxial Creep as a Control on Mercury Intrusion Capillary Pressure in Consolidating Rock Salt

Thomas Dewers, Jason Heath
Geomechanics Department

And

Christi Leigh
Repository Performance Department
Sandia National Laboratories
P.O. Box 5800
Albuquerque, NM 87185-0751

Abstract

The nature of geologic disposal of nuclear waste in salt formations requires validated and verified two-phase flow models of transport of brine and gas through intact, damaged, and consolidating crushed salt. Such models exist in other realms of subsurface engineering for other lithologic classes (oil and gas, carbon sequestration etc. for clastics and carbonates) but have never been experimentally validated and parameterized for salt repository scenarios or performance assessment. Models for waste release scenarios in salt back-fill require phenomenological expressions for capillary pressure and relative permeability that are expected to change with degree of consolidation, and require experimental measurement to parameterize and validate. This report describes a preliminary assessment of the influence of consolidation (i.e. volume strain or porosity) on capillary entry pressure in two phase systems using mercury injection capillary pressure (MICP). This is to both determine the potential usefulness of the mercury intrusion porosimetry method, but also to enable a better experimental design for these tests. Salt consolidation experiments are performed using novel titanium oedometers, or uniaxial compression cells often used in soil mechanics, using sieved run-of-mine salt from the Waste Isolation Pilot Plant (WIPP) as starting material. Twelve tests are performed with various starting amounts of brine pore saturation, with axial stresses up to 6.2 MPa (~900 psi) and temperatures to 90^{o}C. This corresponds to UFD Work Package 15SN08180211 milestone "FY:15 Transport Properties of Run-of-Mine Salt Backfill – Unconsolidated to Consolidated".

Samples exposed to uniaxial compression undergo time-dependent consolidation, or creep, to various degrees. Creep volume strain-time relations obey simple log-time behavior through the range of porosities (~50 to 2% as measured); creep strain rate increases with temperature and applied stress as expected. Mercury porosimetry is used to determine characteristic capillary pressure curves from a series of consolidation tests and show characteristic saturation-capillary pressure curves that follow the common van Genuchten (1978, 1980) formulation at low stresses.

Higher capillary pressure data are suspect due to the large potential for sample damage, including fluid inclusion decrepitation and pore collapse. Data are supportive of use of the Leverett "J" function (Leverett, 1941) to use for scaling characteristic curves at different degrees of consolidation, but better permeability determinations are needed to support this hypothesis.

Recommendations for further and refined testing are made with the goal of developing a self- consistent set of constitutive laws for granular salt consolidation and multiphase (brine-air) flow.

ACKNOWLEDGMENTS

Scott Broome, Greg Flint, and Perry Barrow of the Sandia Geomechanics Laboratory deserve many thanks for their untiring help with instrumentation and calibration. Cliff Howard, Kris Kuhlman and Bwalya Malama provided many interesting discussions contributing to testing design and experimental matrix. Sandia National Laboratories is a multi-program laboratory managed and operated by Sandia Corporation, a wholly owned subsidiary of Lockheed Martin Corporation, for the U.S. Department of Energy's National Nuclear Security Administration under contract DE-AC04-94AL85000.

CONTENTS

FIGURES

TABLES

1. INTRODUCTION

Waste release scenarios from geologic salt repositories, and consolidating backfill and damaged or disturbed salt in particular, involve multiphase gas and brine transport through pore spaces. No data exist presently to parameterize multiphase flow models as a function of degree of consolidation or "healing" in such scenarios (Davis, 1991). This report provides details on a series of salt consolidation and mercury injection capillary pressure tests performed in May 2015 and in late August and early September 2015 with the aim of examining both how consolidation influences multiphase pore transport properties and also how these behaviors may be quantified constitutively. A new experimental capability utilizing titanium oedometers (uniaxial compression cells commonly used in soil mechanics) is used in a testing program to compress granular salt to porosities approaching 2%. Samples exposed to uniaxial compression undergo time-dependent consolidation, or creep, to various degrees. Creep volume strain-time relations obey simple log-time behavior through the range of porosities (~50 to 2% as measured); creep strain rate increases with temperature and applied stress as expected. The resulting consolidated salt samples are then tested via mercury injection capillary pressure (MICP) which produces so- called characteristic curves of capillary intrusion pressure and saturation or degree of pore filling by the non-wetting mercury phase. The characteristic curves are modified to simulate brine-air wetting properties and examined for variations based on consolidation history. The "bundle-of- tubes" model is used to estimate the distribution of pore throats (connecting orifices between larger pores) and shows the progressive shrinking of pore sizes with increasing degree of consolidation. Based on this phase of testing, it appears that the common van Genuchten (1978, 1980) model provides an adequate approximation of the observed characteristic curves. Higher capillary pressure data are suspect due to the large potential for sample damage, including fluid inclusion decrepitation and pore collapse. Data are supportive of use of the Leverett "J" function (Leverett, 1941) to use for scaling characteristic curves at different degrees of consolidation, but better permeability determinations are needed to support this hypothesis. Recommendations for further and refined testing are made with the goal of developing a self-consistent set of constitutive laws for granular salt consolidation and multiphase (brine-air) flow.

Several appendices are included at the end of the report including 1) a technical memo outlining an initial phase of testing exploring benefits and problems of using oedometric consolidation, and 2) a report provided by Porotechnology™ of Houston TX who ran the MICP analysis which gives in depth summaries of the results of MICP.

This report corresponds to UFD Work Package 15SN08180211 milestone "FY:15 Transport Properties of Run-of-Mine Salt Backfill – Unconsolidated to Consolidated".

2. METHODS

2.1. Oedometer Design

This section describes the titanium odeometers used in the compression testing. These were designed at Sandia Laboratories with the purpose of using neutron scattering to investigate changes in pore distributions in samples *in situ* (at stress and temperature conditions, including exposure to gases, chloride brines, and supercritical CO_2). The titanium composition is ideal for use with potentially corrosive chloride brines that precludes use of stainless steel, for example. Figure 1 shows a schematic of the oedometer cells which consist of: a 1" inner diameter pressure vessel or sample cell; two piston assemblies which provide the axial load and are ported to allow fluid access; a lower hydraulic cell which provides fluid pressure against a lower piston assembly and produces the axial sample loading; two over-rings with fittings that provide a sealed pressure port to both the lower and upper piston assembly; an upper and lower plate which ensure alignment and act to secure the configuration to the applied loads; and two tie rods which secure the plates. Photographs of the two oedometers used in this study are shown in Figure 2 and Figure 3. Each oedometer stands approximately 9 inches or ~23 cm high and is rated to 4000 psi or ~30 MPa.

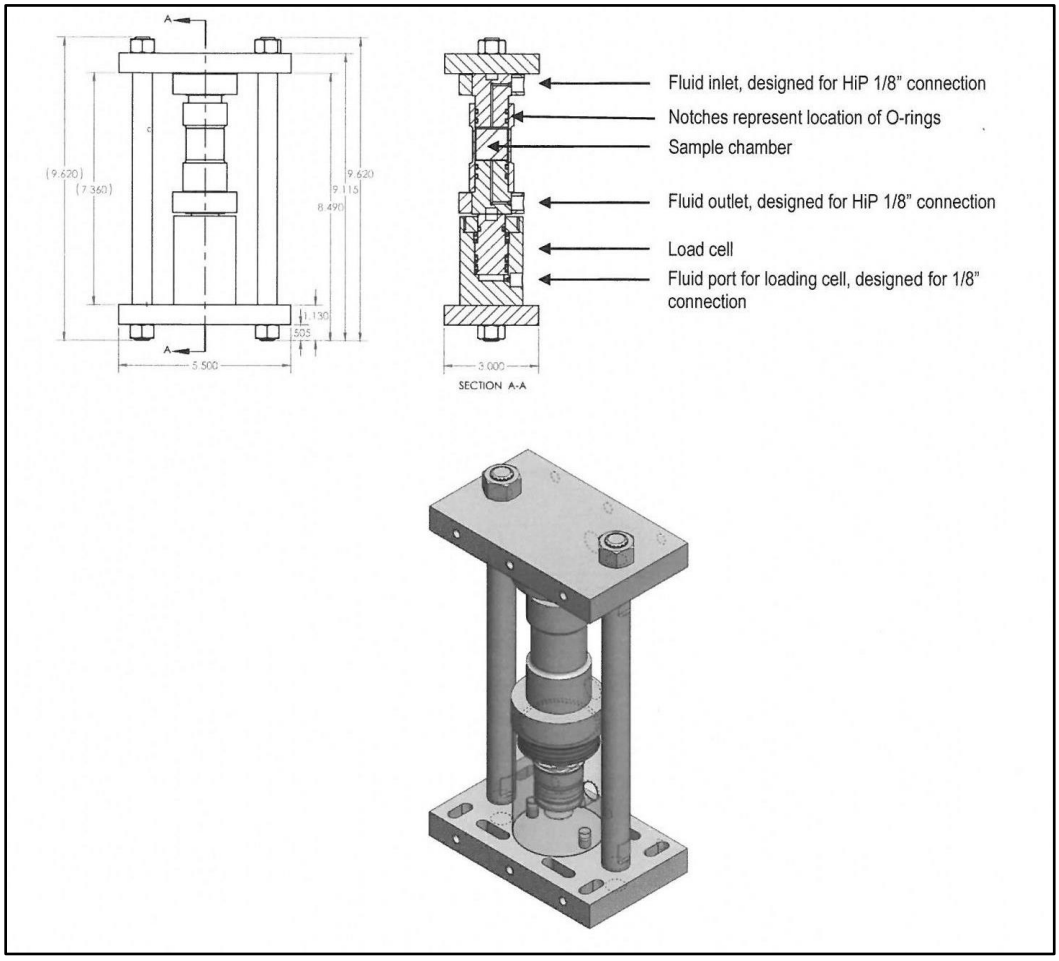

Figure 1. Titanium oedometer design used in the salt consolidation tests.

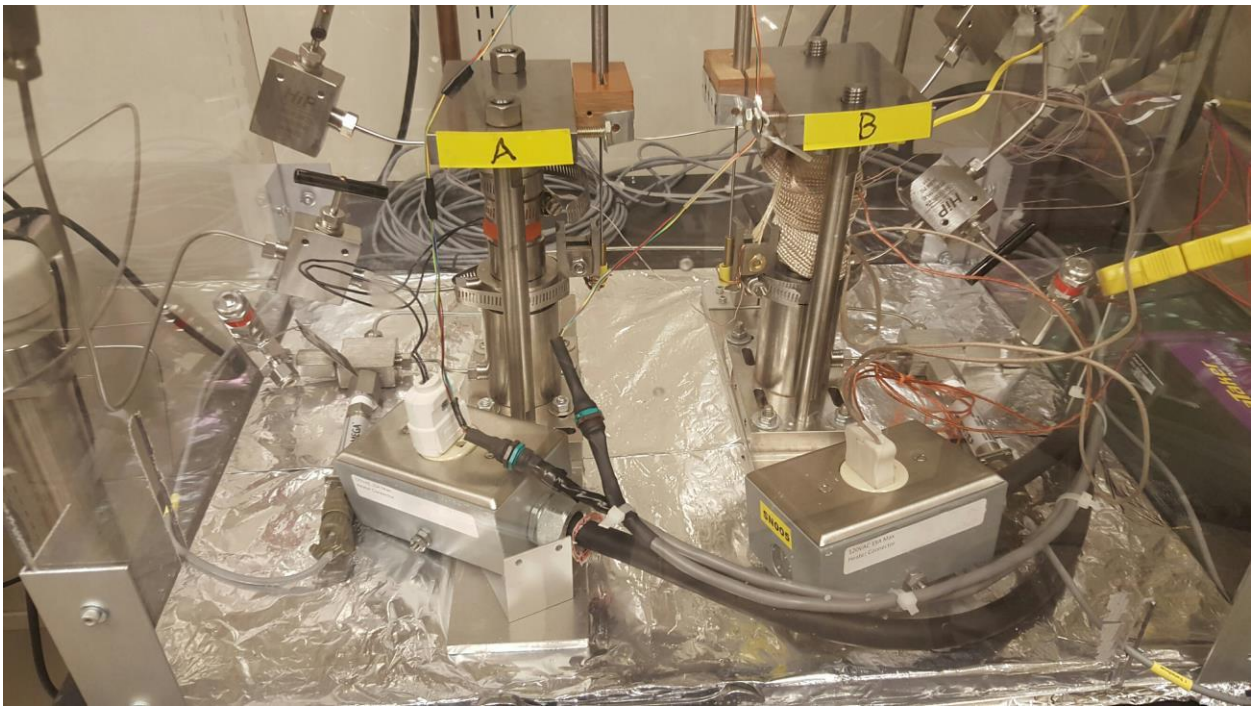

Figure 2. Twin oedometers with mounted LVDTs (in wooden blocks at the top of the cells).

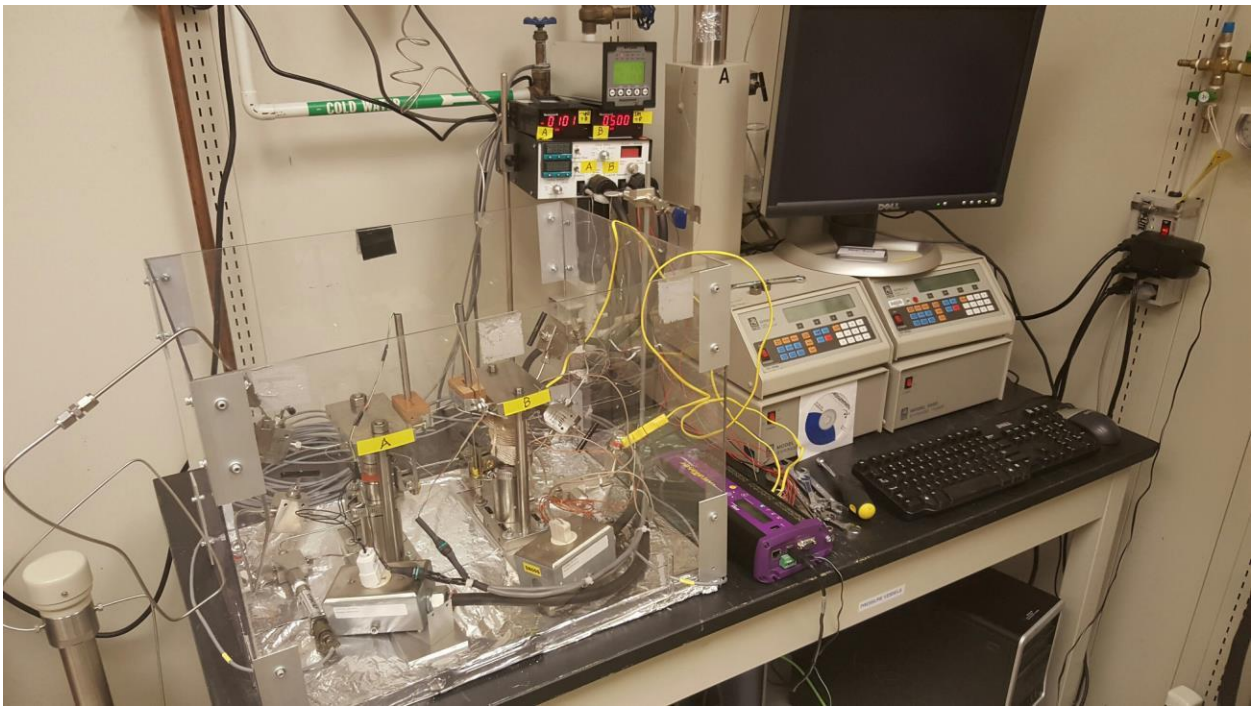

Figure 3. Experimental system, including Teledyne-Isco syringe pumps (at right) used to control the axial pressure and data acquisition system (purple box) and computer.

2.2. Testing System

The testing system shown in Figure 2 and Figure 3 and schematically in Figure 4 provides fluid and pressure control to the oedometer rams, provides flow-through metering and pressure control, permits measurement of axial stress and displacement, and heats and controls temperature of the oedometer sample cells.

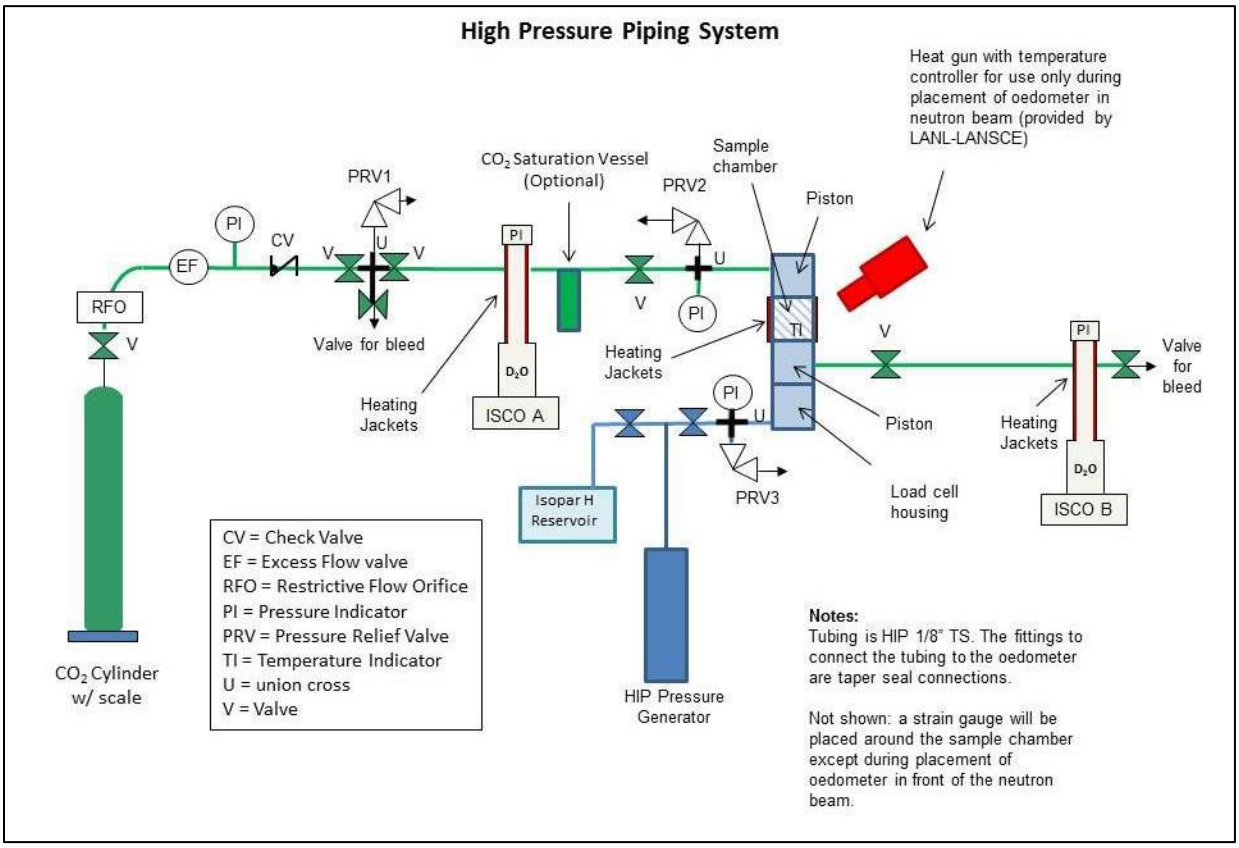

Figure 4. Piping system for full oedometric system with pore pressure control showing safety pressure relief valves and gas flow for permeability determination.

The system includes

- Two Teledyne-ISCO series 500D syringe pumps which can maintain constant flow or pressure and are used to control hydraulic pressure and thus axial stress to the oedometer sample chambers
- Two Teledyne-Sprague series 100D syringe pumps with hastelloy wetted parts which can control flow and pressure for the pore systems. Hastelloy valves and tubing manufactured by High Pressure Inc. complete the pore pressure system.
- Two Omega PX602 pressure transducers and Honeywell GM signal conditioner/meters monitor pressure to the hydraulic cells
- A DT85 16 channel Datataker data logger (the purple box in Figure 3)
- Two Schaevitz/Measurement Specialties MHR Series – Miniature General Purpose AC LVDTMP-2000 LVDTs with an MP2000 Dual Channel LVDT/RVDT Readout/Controller
- Pressure relief valves manufactured by Swagelock provide pressure protection to the system

The pressure transducer/signal conditioners, the LVDTs and signal conditioner, and the data logger are all calibrated either directly by the Sandia National Laboratories Primary Standards Laboratory or by transducers directly traceable to PSL standards.

2.3. Starting Material

Two types of starting material were used for the oedometer tests. For most of the tests, 1.5 kg of < 0.25" screened WIPP run-of-mine salt was obtained from the Sandia Carlsbad office. This is shown in the left hand photo in Figure 5. The second type of material used this size fraction of salt but was dry loaded over a few minutes to 900psi or 6.2 MPa. This resulted in plastic strain and grain size reduction or comminution (shown in the right hand photo in Figure 5). This was done for two tests in order to maximize piston stroke within oedometers such that little stroke would be used to compact the material plastically to 6.2 MPa.

A brine solution was prepared by dissolving ~50 g of salt in ~250 mls of distilled water and stirring on a hot plate overnight. The resulting solution was filtered to remove clay impurities and remaining undissolved salt. This permeant was applied to the solid salt prior to testing.

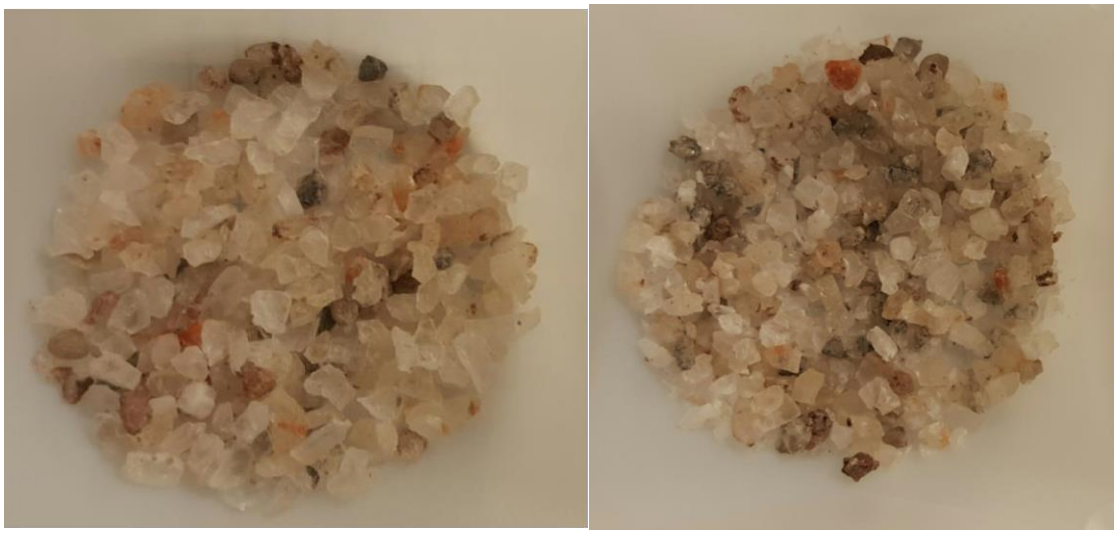

Figure 5. Starting material for consolidation tests including WIPP run-of-mine salt sieved to less than 0.25" (0.64 cm; left photo) and the same material loaded nearly instantaneously to 6.2 MPa (900 psi) under dry conditions (right photo).

3. RESULTS

3.1. Salt Consolidation

3.1.1. Phase 1 Testing

Salt consolidation experimental testing was done in two phases. The first phase was performed in May 2015 and done to assess the performance of the oedometer systems. Results of this testing are summarized in Appendix A. Two tests from this series are included in the present discussion. Test 3 (Appendix A, page 4) was the most successful test of the series, achieving the most extensive consolidation over a period of about 20 hours at 90°C and 136 psi (0.94 MPa) effective axial stress with 2% added brine by weight. Test 4 was done with pores fully saturated with brine. Approximately 17 g of salt was loaded into the vessel with an excess of brine (distilled water chemically saturated with WIPP salt at room temperature). The salt was compacted over a period of about 21 hours at 90°C and 136 psi (0.94 MPa) effective axial stress. The exit port of the upper pore pressure line leading to the ISCO pore pump was seen post-test to be blocked by salt precipitation, and it is thought that this salt plugged the pore line from hot brine that was squeezed from the sample early in the test and precipitated salt upon cooling in the exit pore line. The sharp drop in creep rate at about 1 PM on 5/13/2015 (Appendix B Figure 5) could reflect a lowering of creep rate as the sample moved from drained to undrained conditions. Interestingly a large vug developed at some point during the run that did not drain by gravity at the end of the test, seen in Appendix B Figure 1E. The vug may have been a pocket of overpressured brine that developed under these undrained conditions. The remaining salt

examined by visual inspection (Appendix B Figure 1E) showed that compaction via expression of pore fluid brine into the large vug pore appears to have continued throughout the duration of the test. Mercury porosimetry (MICP) results shown below suggest that tests 3 and 4 samples have very similar pore structures and capillary pressure characteristic curves.

3.1.2. Phase 2 Testing

The second phase of testing includes 8 oedometer tests summarized in Table 1. The testing matrix was designed to achieve different levels of consolidation in order to compare capillary pressure variations with degree of consolidation.The end products were used for MICP testing and are shown in Figure 6. We describe each of these tests in numerical order.

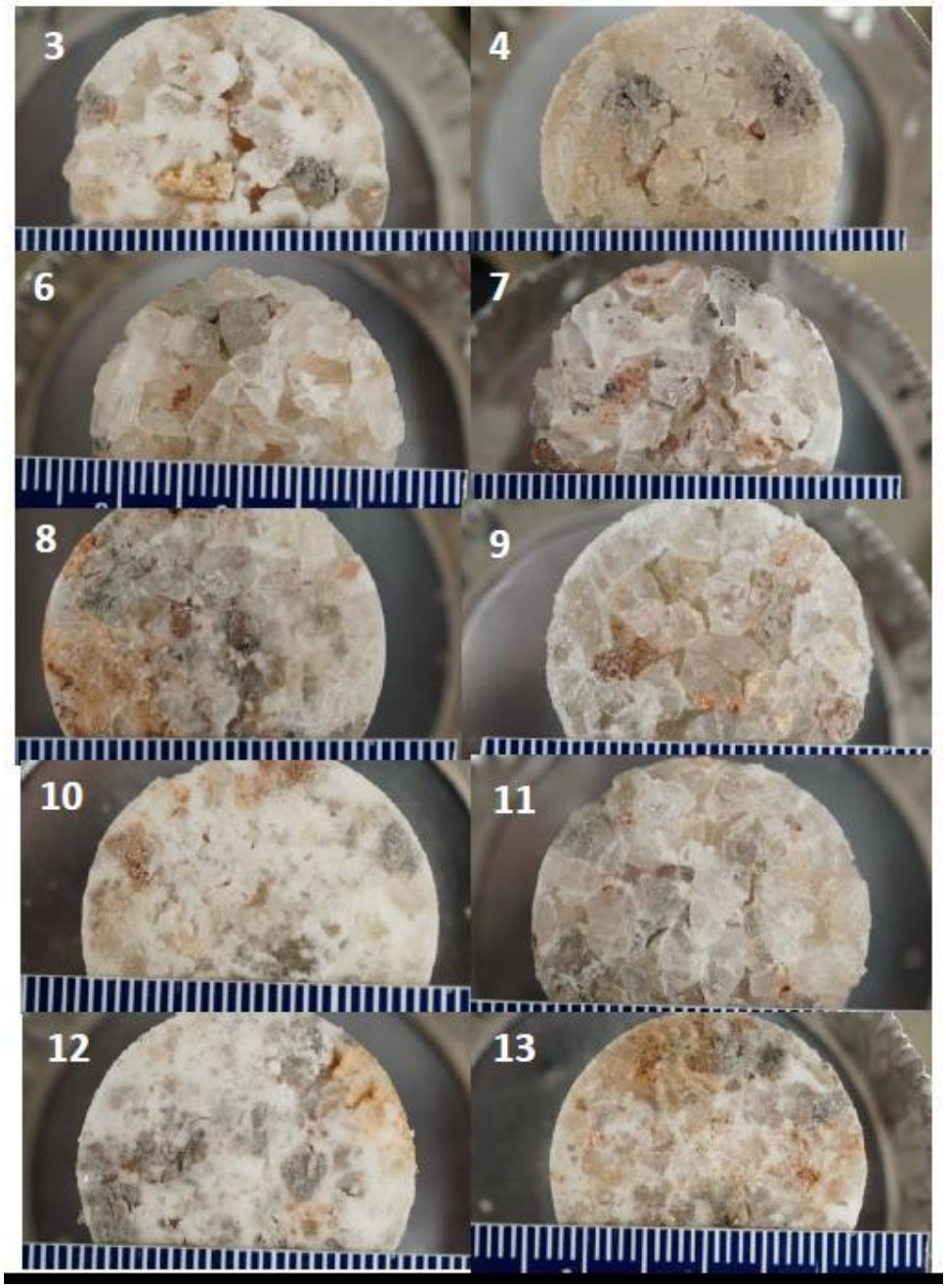

Figure 6. Consolidated salt samples used for mercury porosimmetry. These photos were taken by PoroTechnology staff shortly after the samples arrived at their laboratory showing that the delicate salt samples survived shipping.

Table 1. Salt consolidation sample initial and final conditions

Test	T (°C)	Duration (hr)	Axial Stress (MPa)	Initial Weight (g)	Initial Height (cm)	Max Displacement (cm)	ϕ, initial	ϕ, final (prior to unloading)
6	25	90	1.7, 3.4, 5.2	17.13	3.086	0.679	0.49	0.35
7	90	90	1.7, 3.4, 5.2	16.98	2.923	0.906	0.47	0.23
8	91	25	6.2	16.13	2.664	0.585	0.45	0.29
9	85	25	6.2	16.50	2.999	0.881	0.49	0.29
10	92	24	6.2	9.229	1.588	0.742	0.47	0.01
11	86	24	6.2	16.62	2.852	0.857	0.47	0.24
12	88	20	6.2	20.45	2.830	0.855	0.34	0.05
13	95	20	6.2	12.28	1.895	0.735	0.41	0.03

3.1.2.1. Tests 6 and 7

These two tests are identical except for temperature. Test 6 was run at ambient temperature, circa 25 ^{o}C, whereas Test 7 was run at 90^{o}C. Both samples were subject to a stress stepping protocol with ~ 24 hours at 1.5 MPa axial stress, 24 hrs at 3.6 MPa, and 48 hours at ~ 5.2 MPa. The displacement curves and stress history are shown in Figure 7. Test 7, at the higher temperature, experiences more consolidation (total displacement of ~ 1 cm), with a porosity change from 0.47 to 0.23 (or 47% to 23%) prior to elastic unloading. For Test 6, porosity changes from an initial amount of 0.49 (49%) to a minimum of 0.35 (35%) prior to elastic unloading. The porosity changes including elastic unloading are shown in Figure 11.

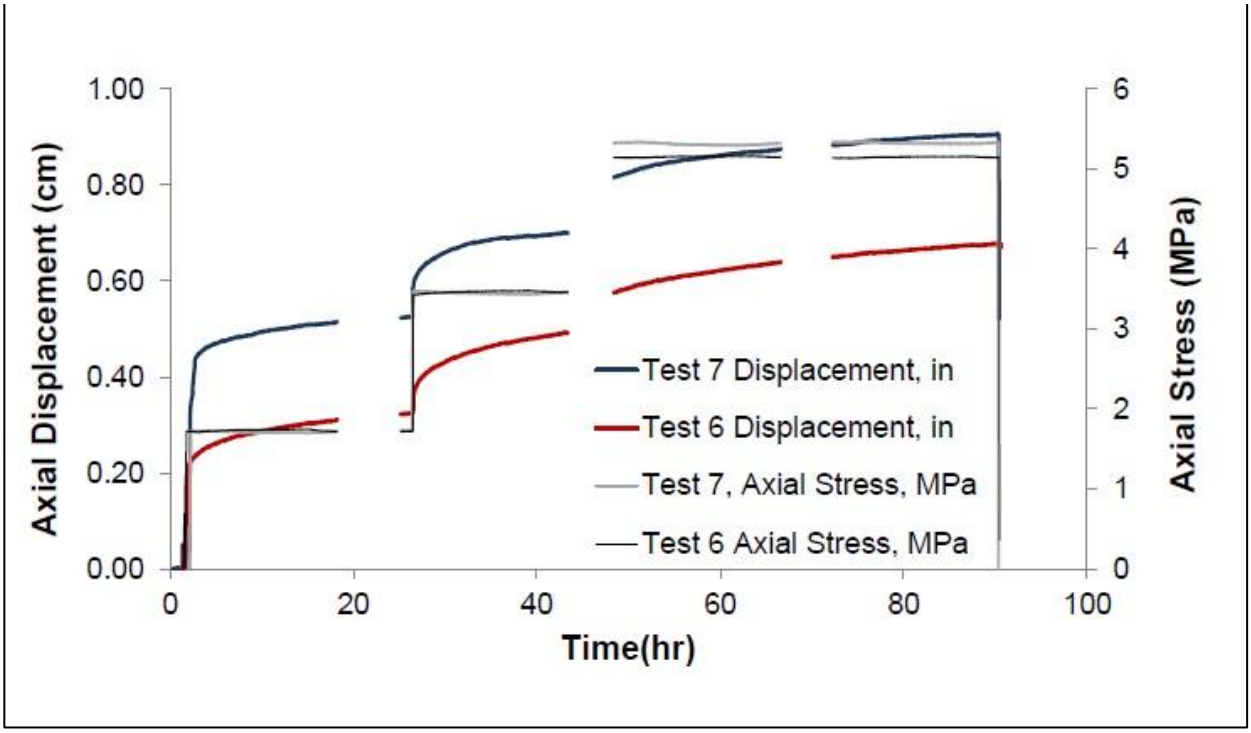

Figure 7. Axial stress (grey lines) and axial displacement (red and blue lines) versus time for Tests 6 and 7.

3.1.2.2. Tests 8 and 9

Tests 8 and 9 are identical tests loaded directly to 6.2 MPa axial stress over a duration of 25 hrs. The initial starting length of these tests, and the extensive plastic axial strain experienced by loading to this stress level resulted in the pistons for both tests achieving maximum stroke relatively early in the loading history, perhaps 4 or 5 hours once constant stress had been achieved. The early data logger data was lost at the conclusion of these tests with only the last ten hours of displacement data saved, which showed no further consolidation during the final ten hours of each test. The initial and final porosities (~0.29 or 29%) and loading and unloading histories are known. The discrete stress-displacement data are shown for Test 8 (Test 9 values are almost identical and are omitted for clarity) in Figure 11 for completeness and are used in the compilation of MICP data.

3.1.2.3. Tests 10 and 11

Tests 10 and 11 were a repeat of the somewhat failed Tests 8 and 9 and loaded to 900 psi (6.2 MPa) for 24 and 7 hours respectively. To handle the limited stroke of the oedometers, Test 10 used a spacer configuration so that less stroke would be taken up with plastic deformation of the salt upon loading to the 6.2 MPa axial stress. 6 hastelloy frits (manufactured by Valco) were set within the oedometer sample chamber so that any deformation is accommodated by the salt alone (save for elastic deformation of the frits themselves, which we ignore here for simplicity). The displacement of both tests with time is shown in Figure 8. Test 11 experiences more axial displacement (as it is the longer specimen) but is shorter in duration and the porosity changes from 0.47 (47%) to 0.24 (24%). Test 10 measured porosity decreases to near zero (light blue curve in Figure 11 below) but visual inspection shows that some salt flowed up between the interior walls of the oedometer and the lower most hastelloy spacer (Figure 9). The extent to which this affects the final calculation of porosity is unknown but the final amount of consolidation and thus porosity estimate for test 10 is overestimated.

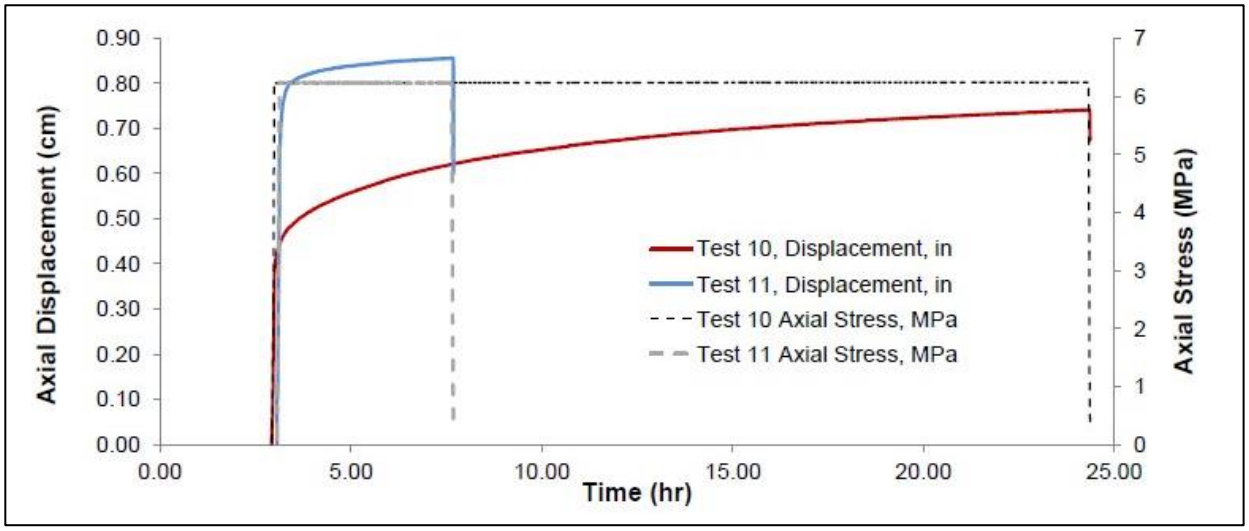

Figure 8. Axial stress (grey lines) and axial displacement (red and blue lines) versus time for Tests 10 and 11.

Figure 9. Photograph of final test sample 10 along with hastelloy spacers at the end of consolidation testing. Note the creep of salt along the edges of the spacers, which adds error to estimates of final porosity as shown in Figure 12.

3.1.2.4. Tests 12 and 13

Tests 12 and 13 were a slightly different attempt to handle the limited stroke of the pistons by pre-consolidating the samples by loading them to 6.2 MPa under dry conditions. In Test 12 the full oedometer cell volume was loaded with a pre-consolidated salt sample and in Test 13 thastelloy frits were used. Results of consolidation are shown in Figure 10. Porosities change from 0.35 (35 %) and 0.41 (41%) for tests 10 and 11 respectively to 0.05 (5%) and 0.03 (3%).

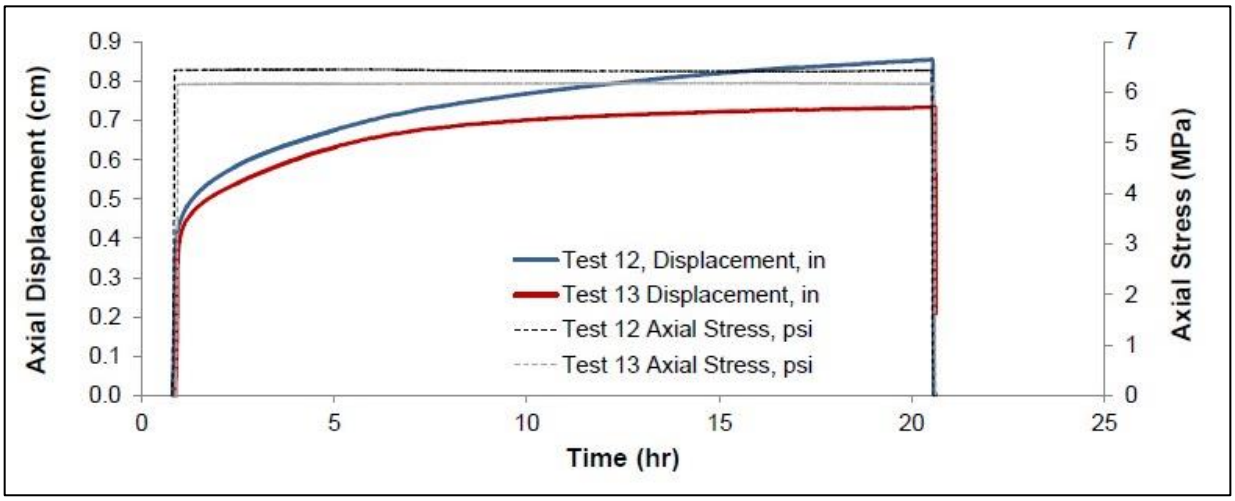

Figure 10. Axial stress (grey lines) and axial displacement (red and blue lines) versus time for Tests 12 and 13.

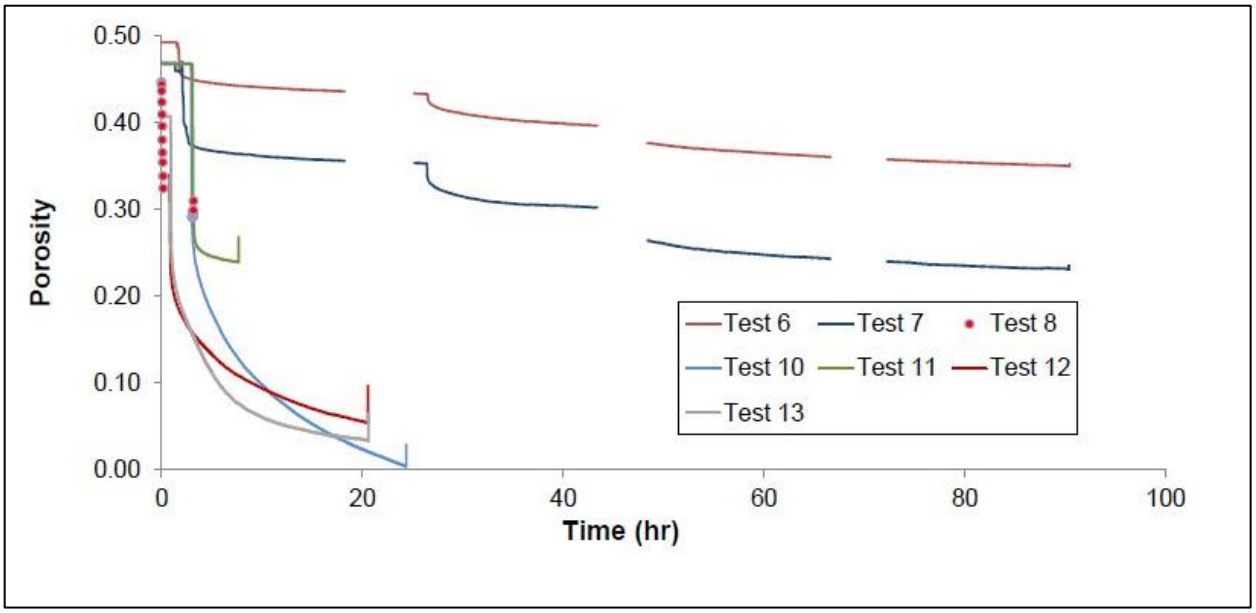

Figure 11. Porosity of salt samples undergoing oedometric compression. Only initial consolidation and unloading data are available for Tests 8 and 9. Test 9 results are nearly identical to Test 8 results and so are not shown for clarity.

3.1.2.5. Elasto-Plastic Consolidation

Consolidation curves (plotting void ratio or ratio of pore to solid volumes as a function of ln(axial stress) for selected test results deformed to 6.2 MPa axial stress are shown in Figure 12; creep portions of the curves are the vertical portions at right. This is a common analytical method used in soil mechanics where the break in slope in initial loading is interpreted as a change from elastic to plastic consolidation, the latter being termed the primary consolidation line. For salt this type of analysis may not be as straightforward as creep undoubtedly occurs during plastic deformation and there is no clear break in slope. In addition in elasto-plastic experiments we would interpret the unloading portions of the curves as elastic, however large change in stress occur without discernable changes in axial stress during unloading. The single-acting ram design of the oedometer design likely precludes elastic analysis during unloading; this requires further analysis beyond the scope of this report.

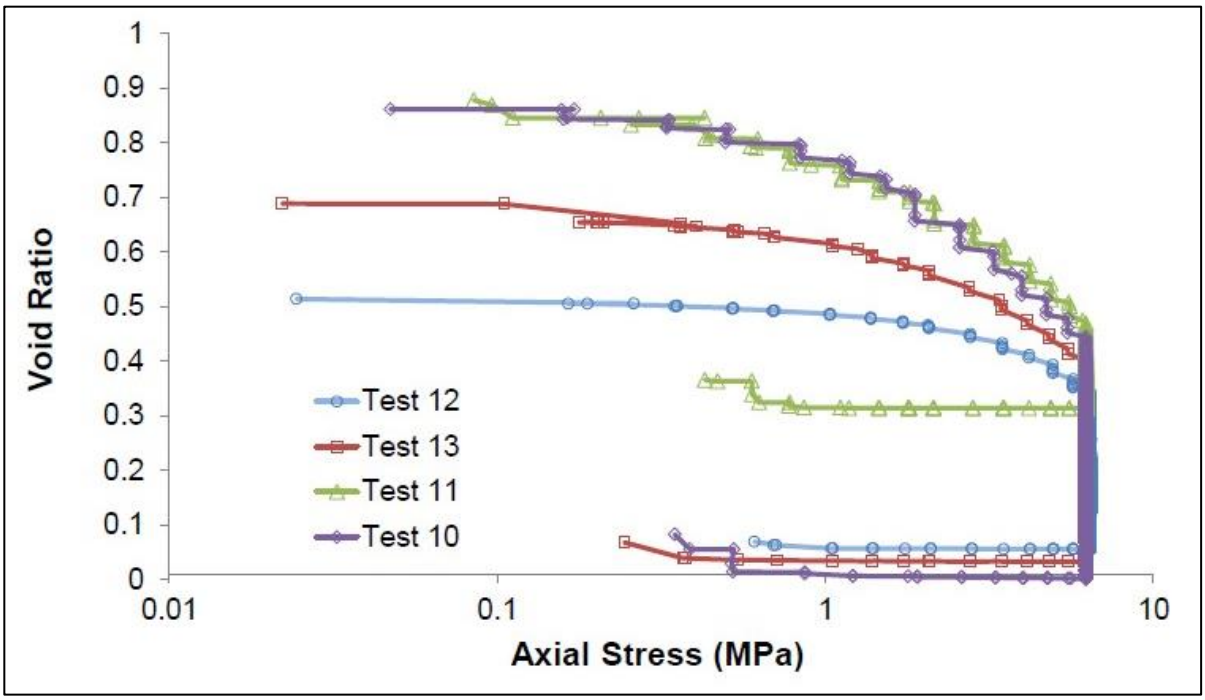

Figure 12. Consolidation curves, in the form of void ratio versus log(axial stress) (as is common in soil mechanics) for selected tests. The vertical lines display creep at constant applied axial stress.

3.2. Creep Behavior

"Creep" or viscous deformation is the time-dependent strain that occurs during constant loading conditions. So-called "brittle creep" in porous rocks can occur by multiple mechanisms; important mechanisms are solution transfer or "pressure solution" and water-assisted chemically- and thermally-activated sub-critical crack growth and healing (Ko and Kemeny, 2011; Brantut et al., 2012; 2013). A simple rate expression for this type of deformation can be expressed in the form (Scholz, 1968; Dewers and Hajash, 1995, Brantut et al., 2013):

$$\varepsilon - \varepsilon_0 = C_1 \ln(1 + C_2 t) \qquad (1)$$

where ε is volume strain, ε_0 is volume strain at time zero, t is time, and C_1 and C_2 are stress and temperature dependent coefficients. Note that this expression only allows for what are termed primary and secondary creep (Scholz, 1968) and not the acceleration of strain in the so-called tertiary creep phase observed in the presence of high triaxial loads (Brantut et al., 2013).

Following Dewers and Hajash (1995), eqn. 1 yields a form of strain rate as:

$$\frac{d\varepsilon^{vs}}{dt} = \frac{C_1}{C_2^{-1} + t} \tag{2}$$

where C_2 carries a stress dependence which won't be explored here.

It appears that the log-time creep law is capable of describing the volumetric creep rates of salt under these conditions to a reasonable degree (Figure 13).

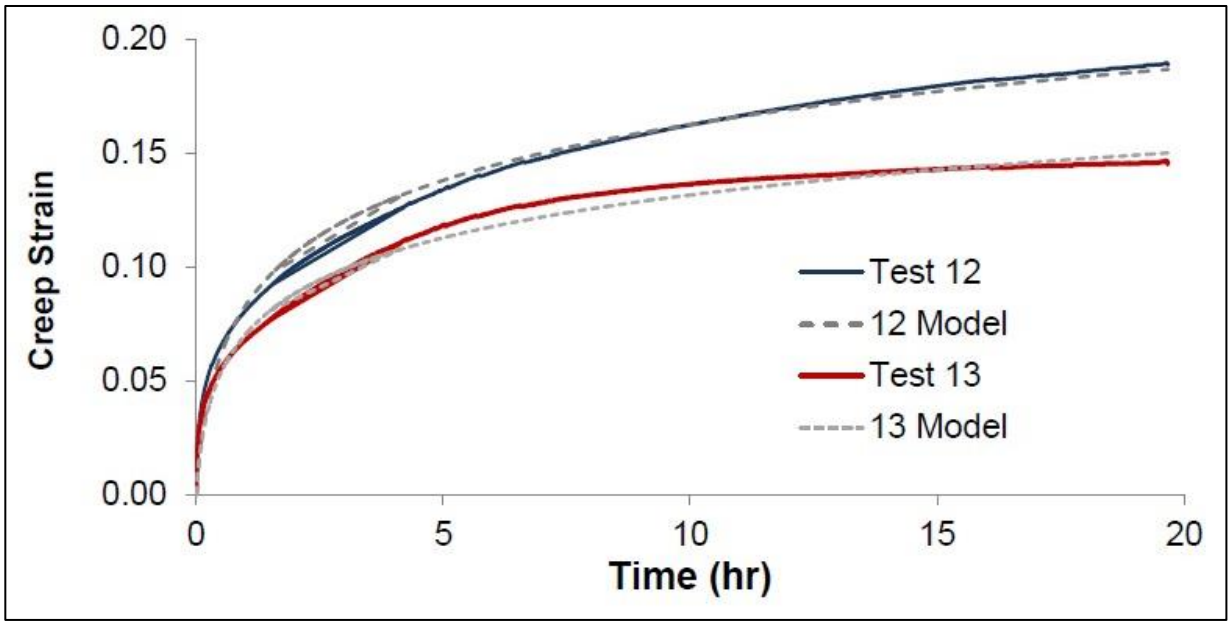

Figure 13. Creep volume strains compared to simple fits from the model in equation 1 for two tests that show consolidation from ~45% porosity to less than 5% porosity. (Test 12: {C1, C2} = {0.0360, 9}; Test 13: {C1, C2} ={.0272, 12}).

3.3. Mercury Intrusion

3.3.1. Motivation and Background on Mercury Intrusion Capillary Pressure Measurements

The MICP measurements involve injection of the "non-wetting" mercury into a consolidated salt sample from low to high (i.e., 60,0000 psia or ~ 400 MPa) pressure. Poro-Technology in Sugar Land, TX, performed the MICP tests on a Micromeritics AutoPore IV 9500 V1.07 instrument (Poro-Technology is a subsidiary of Micromeritics^{TM}). Salt samples are heated to 100^{o}C, and placed under vacuum prior to the measurements. Data produced include incremental (and cumulative) volumes of mercury injected into the penetrometer vessel containing the rock sample and the corresponding pressures. The salt samples we provided to Porotechnology were too large to fit into their penetrometry vessel (just slightly over 1 inch) and so the samples were broken into smaller pieces using a razor knife. Weights of resulting samples used in the analysis are given in Table 2. This appeared to work well except for sample 8, which was fairly friable and broke into several small chunks, one of which was tested via MICP.

3.3.2. Data in Appendix B Spreadsheets and Conversion to Air-Brine Systems

Poro-Technology assembled the raw MICP data in an Excel spreadsheet form, which includes with analysis and plots that are standard for use of these types of data by the petroleum industry. We share these spreadsheets here in PDF format, with minor additions given in the "SPL INFO" worksheet (Appendix B).

A closure correction is a critical first step in analyzing MICP data. It refers to the pressure and the corresponding cumulative mercury volume during a MICP test when mercury first enters the pore space of a sample. After filling of the penetrometer vessel containing a rock sample, mercury is injected into the sample at pressure. The mercury can conform to the surface roughness of the sample and walls of the bulb prior to entering the pores of the sample (see Sigal, 2009). Thus, intrusion volumes are measured that do not represent complete volumes of pore space. The closure volume of mercury is subtracted from the cumulative mercury intrusion volumes so that the data only represent volumes of sample pore space. Many methods for determining closure pressure exist (Katz and Thompson, 1987; Dullien, 1992; Sigal, 2009). For repeatability and to reduce subjectivity, and since non-intrudable blanks for corrections were not used, estimation of the closure pressure are based on a compressibility method (Colombo and Carli, 1981; Almon et al., 2008). For the salt samples, it was decided to not apply a closure correction on the advice of Poro-Technology staff.

The "RESULT" worksheets contain the majority of calculations needed for plots of pore size distribution and other curves. "bc" and "ac" stand for "before closure" and "after closure", respectively. The spreadsheets contain complementary data to previous memos on petrophysical properties of the salt samples. The "SPL PPGD" worksheets provide MICP porosity, bulk density, grain density, and calculated permeability.

Conversion of intrusion pressure to pore throat diameter used a "bundle of capillary tubes" model via the Washburn equation (version of the Young-Laplace equation; Washburn, 1921; Dullien, 1992):

$$d = \frac{4\gamma|\cos\theta|}{P_c} \tag{3}$$

where d is the pore throat diameter of the modeled cylindrical pores, γ is the surface tension of mercury (or in general the interfacial tension between the non-wetting and wetting fluids), θ is the mercury-air/vacuum-rock contact angle, and P_c is the capillary pressure or in this case the mercury intrusion pressure (pressure difference between non-wetting and wetting fluids). Values used for contact angle and the mercury surface tension were 140° and 0.480 N m^{-1} (Pittman, 1992), respectively.

Data end-users can make changes to the worksheets to convert from the mercury-air/vacuum system to the air-groundwater system using this equation:

$$P_{groundwater/air} = P_{air/mercury}\frac{\left(\gamma_{groundwater/air}\cos\theta_{groundwater/air}\right)}{\left(\gamma_{air/mercury}\cos\theta_{air/mercury}\right)} \tag{4}$$

where P represents the capillary pressure for the system in question labeled by the subscripts, and γ and θ represent interfacial tensions and contact angles. To convert to an air-brine system, we used a value of 0.0728 N/m for γ and 0.0 for the brine-air contact angle (Bwalya Malama, 2015, personal communication).

Table 2. Mercury intrusion capillary pressure (MICP) starting conditions and results

Test	Sample Weight (g)	Bulk Density (g/cm^3)	MICP Porosity (%)	MICP Permeability (md)	Median Pore Throat Dia (micron)
3	6.981	2.113	8.76	223.5	34.10
4	6.489	2.011	9.23	788.7	69.20
6	9.434	2.129	4.6	70.79	18.18
7	6.124	2.028	6.65	49.93	13.35
8	3.573	2.147	5.62	19.23	11.56
9	9.779	2.023	7.34	70.80	18.68
10	5.252	1.950	11.3	131.4	19.57
11	10.40	2.085	4.27	50.10	28.33
12	10.52	1.969	9.26	177.4	25.77
13	5.469	2.073	5.93	37.10	15.12

3.3.3. Characterization of Pore Structure and Flow Characteristics

Figure 14 plots capillary pressure data (shown as a function of wetting-phase saturation, equal to 100 minus mercury saturation expressed as a percent of total pore volume fraction) and pore throat size distributions (PSD)—incremental mercury saturation (i.e., volume of mercury intruded during a particular pressure step divided by the total intruded mercury, corrected for closure) versus pore throat diameters. A selected set of test results are shown in Figure 15. The majority of the salt samples have modal/peak values of approximately 30 μm or less (Table 2). Note that the mercury method by its nature excludes pore diameters larger than 100 microns and so truncates the pore size distribution at about 100 microns. Most of the curves indicate bimodal throat sizes with a second peak at of 0.1 μm or smaller. In Figure 15 (left plot) sample 6, which was run at 25 degrees C, has a peak at about 100 microns while sample 7, which has compacted to a great degree at 90 degrees C, shows a shift to the left with a peak at about 10 microns, suggesting a not-surprising result in that consolidation results in a shift of the pore size distribution to smaller pore throat sizes. The distributions for the samples which experienced the most consolidation (10, 11, 12, and 13) suggest a shift to an even smaller pore size distribution with a growing peak at about 3 microns. It is not known what aspect of pore connectedness or topology these changes reflect, but there does seem to be a clear progression to smaller pore throats following consolidation that should have a large influence on absolute and relative permeability.

One interesting aspect these results show is a large peak at ~ 0.005 microns for essentially all of the samples. We could attribute these to perhaps influences of mercury at higher pressure in affecting some sort of salt deformation (pore collapse or decrepitation of salt fluid inclusions). Poro-Technology staff is of the opinion (Ben Harrell, personal communication, September, 2015) that the salt remained intact and did not show characteristics of disaggregating at the higher pressures, based on their experience. It is not known if these nanometer-sized pores reflect an aspect of intragranular porosity in the salt, some kind of influence of the small amount of clay in the sample, or perhaps some sort of grain boundary porosity. That this small distribution is most present for sample 6, which experienced consolidation at the lowest temperatures and stresses (Figure 15, left hand curve) and is smaller for samples which experienced more consolidation, is that this nano-porosity is an existing feature in the provided salt and is progressively lost with consolidation.

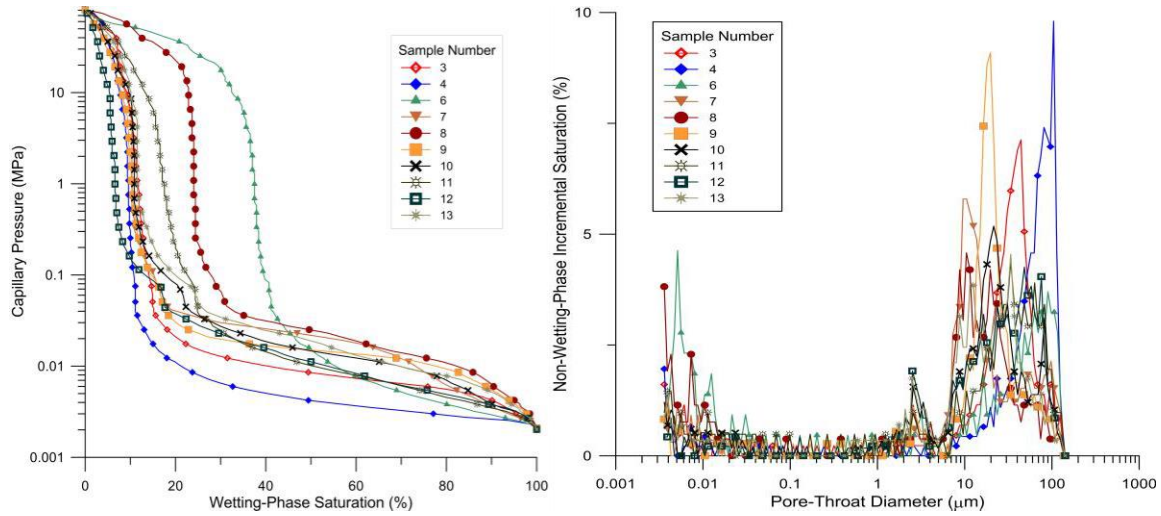

Figure 14. Capillary pressure data and pore-throat distribution plots for ten salt tests.

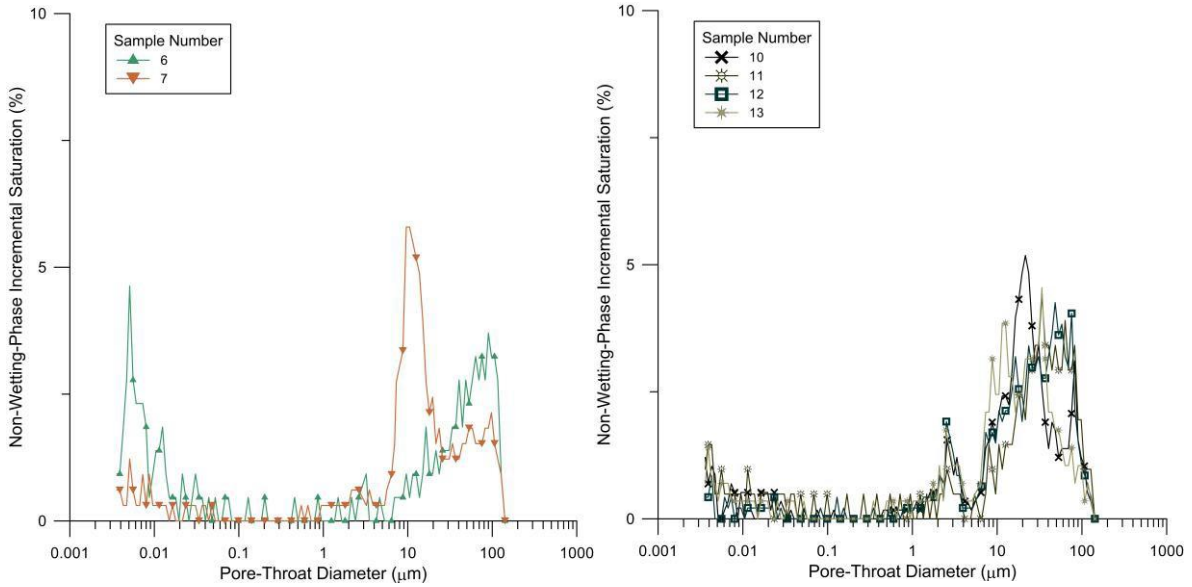

Figure 15. Pore throat size distributions for selected experimental data discerned from capillary pressure curves assuming the "bundle-of-tubes" model. The left-hand plot is for samples 6 and 7; the right-hand plot is for samples 10, 11, 12, and 13.

4. DISCUSSION

4.1. Towards a Predictive Capability

While the above results are preliminary and do not provide a statistically valid sampling, it is nevertheless of interest to examine the potential for quantifying results or the oedometer and MICP testing in the form of constitutive laws. As an example in Figure 16 we have fit capillary pressure data using the parametric van Genuchten formulation for capillary pressure (van Genuchten, 1980), as implemented in many numerical simulators. This formulation follows:

$$P_{cap} = -P_0\left([S^*]^{-1/\lambda} - 1\right)^{1-\lambda}, \quad (5)$$

$$S^* = \frac{S_l - S_{lr}}{S_{ls} - S_{lr}}, \quad (6)$$

where P_{cap} is the capillary pressure or difference in pressure between the nonwetting and wetting phases, subject to the restriction that $-P_{max} \leq P_{cap} \leq 0$; P_0 is the entry pressure of the nonwetting phase; S_l is the saturation of the wetting phase; S_{lr} is the residual wetting phase saturation; S_{ls} is taken to be unity; and λ is a parameter related to the shape of capillary pressure curve. As a cursory examination of the applicability of this function to salt consolidation, Figure 16 shows example fits of equation 5 using λ of 0.524; P_0 equal to 0.01 MPa for tests 13 and 8, 0.002 for test 4, and 0.004 for test 6; S_{lr} decreases with extent of consolidation and we used values of 0.365, 0.23, 0.11, and 0.09 for tests 6, 8, 13, and 4. These values provide a reasonably good fit to the experimental data.

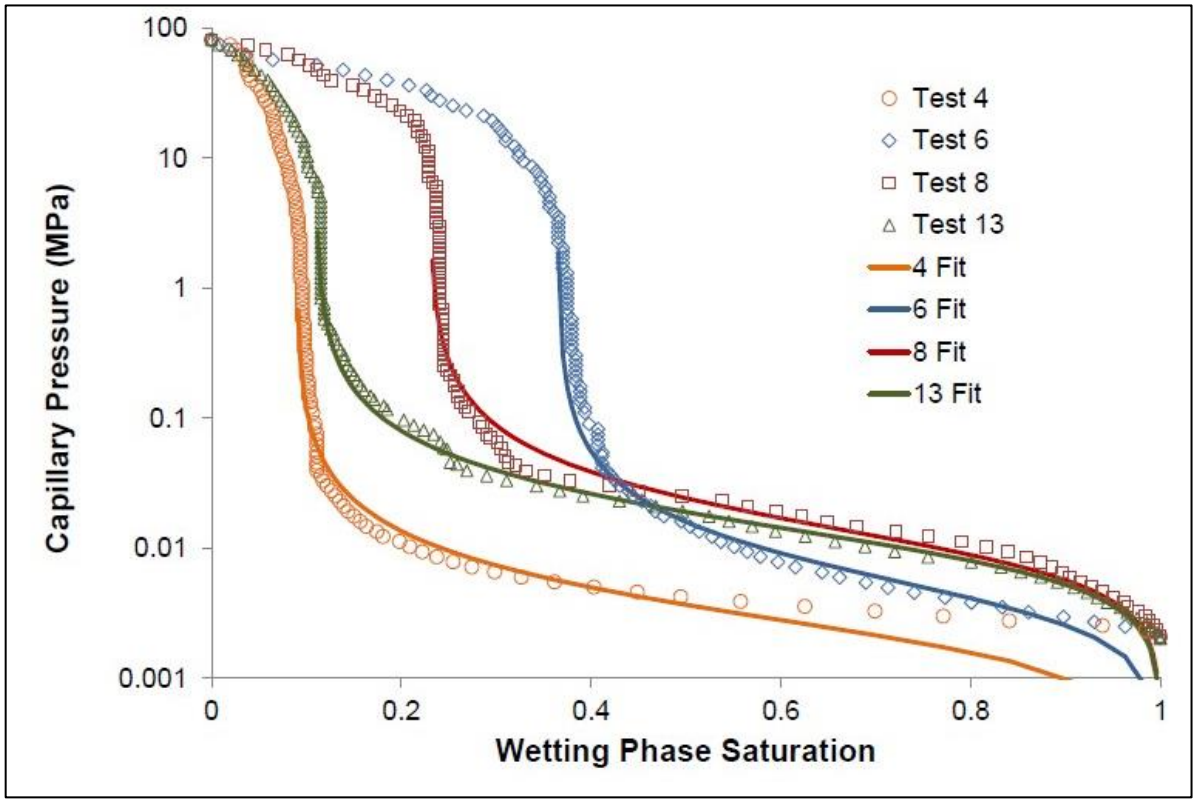

Figure 16. Selected experimental capillary pressure curves along with example "fits" to the van Genuchten (1978, 1980) capillary pressure formulation.

4.1.1. Leverett-J Scaling

The Leverett (1941) "J" method uses a ratio of permeability to porosity as a characteristic length in the function

–

$$J(S_l) = \frac{P_{cap}}{\sigma cos\theta}\sqrt{\frac{k}{\varphi}} \quad (7)$$

where k is single phase permeability and ϕ is porosity. For modeling purposes this function is often used in reservoir simulation to account for heterogeneity from grid block to grid block Saadatpoor et al. (2007). Here we want to make an assessment of the applicability of the J function to account for changes in capillary pressure as salt consolidates. If we can model porosity changes with consolidation via a model such as equation 1 and model permeability using changes in pore throat aperture as shown in Figure 15, the J function enables one to calculate the characteristic capillary pressure curves as a function of evolving porosity and permeability (assuming interfacial tension and contact angle do not vary with consolidation) via

$$P_{cap,j} = P_{cap,j}\sqrt{\frac{k_i\varphi_j}{k_j\varphi_i}} \quad (8)$$

The Levertt J function determined from the Porotechnology analysis for all samples is shown in Figure 17. This is a somewhat imperfect application as the higher porosity samples (e.g. 6, 11, and 8) do not have an accounting of the complete pore volumes for pore throats larger than ~100 microns and the permeability values are estimates from the mercury intrusion and are not corrected for temperature. Nonetheless the collapsing of the remaining curves on top of each other does suggest that the use of the J function in numerical models holds some promise to account for increasing consolidation on capillary pressure characteristic curves.

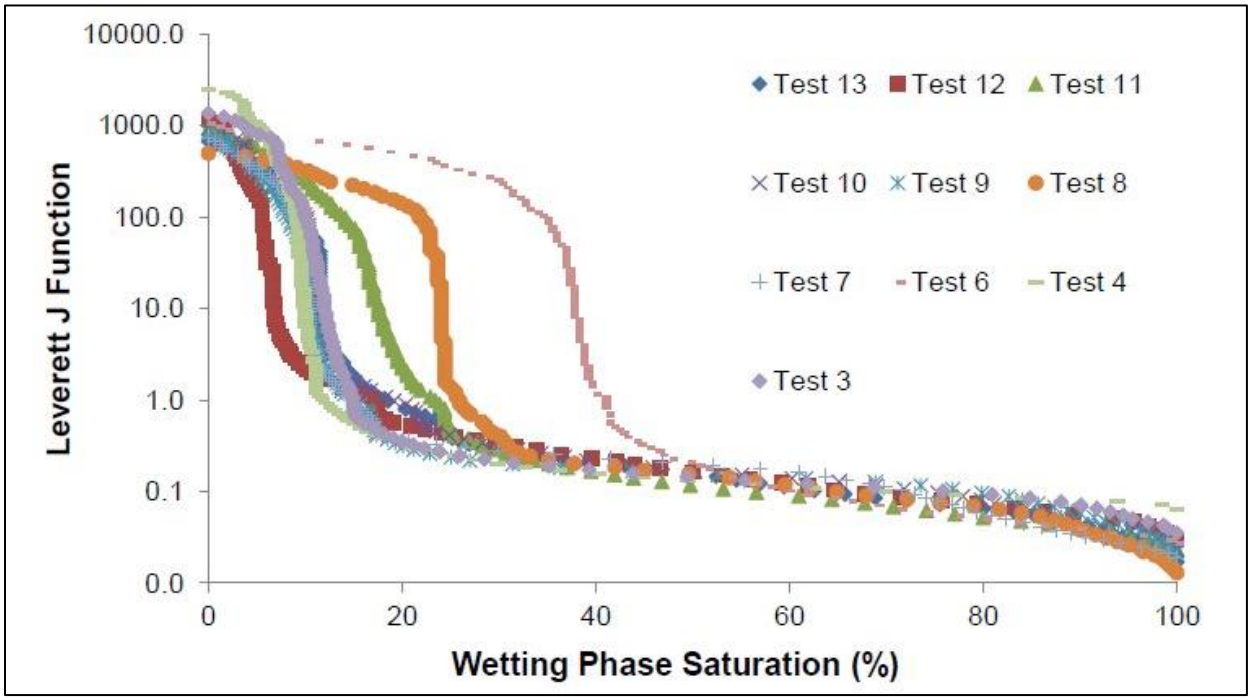

Figure 17. The Leverett J (Leverett. 1941) function applied to all consolidation tests.

5. CONCLUSIONS AND RECOMMENDATIONS

5.1. Conclusions based on the existing data set:

1. A logarithmic-in-time creep behavior consistent with other primary volumetric creep studies appears to fit the creep portions of the testing exceptionally well. The law needs to account for the small but probably significant differences in starting pore

volumes between samples, axial stress, grain size, and temperature.

2. The often-used Van Genuchten (1978, 1980) formulation for capillary pressure as a function of wetting phase saturation appears to provide a good description of consolidating salt behavior, at least at and around pressures equivalent to confining stresses experienced by the samples during testing. An extension such as the one proposed by Webb (2000) applicable at higher pressures and non-wetting phase saturations could be used to describe the higher pressure behavior if of interest, but it is not known what kind of sample damage (and resulting modification of pore structure) may be occurring at those high pressures.
3. The Leverett-J function holds potential to describe evolution of capillary pressure as a function of evolving permeability and porosity as granular salt consolidates. This function is often used in the petroleum industry to account for heterogeneity in porosity and permeability and is based on the bundle-of-tubes capillary model of porous media. It would require good determinations of porosity and permeability (and in particular, the temperature dependence of the latter) as a function of consolidation to truly test its applicability to consolidating porous media.

5.2. Recommendations for future testing:

1. The dual oedometer system is small enough and designed such that a better precision temperature control could be obtained by placing the system inside an oven (excepting ISCO pumps).
2. This method presents the possibility of development of a self-consistent set of constitutive equations or "rate laws" including axial creep, capillary pressure, and relative permeability. The present system could be easily modified to permit measurement of air or nitrogen relative permeability as a function of brine saturation during consolidation. One complication is of course that brine saturation in consolidating pore spaces increases as pore volume decreases with consolidation. Care should be taken to ensure that gas used to determine relative permeability is brine-saturated prior to use.
3. Samples should be dried under vacuum and then at temperature immediately following conclusion of testing to prevent any further precipitation of salt. Air (or better, nitrogen) permeability should be determined both pre-compaction and post-compaction on the sample when pores are free of brine.
4. Petrographic examination of samples needs to be conducted in concert with other (destructive) techniques such as MICP. Due to the nature of the mercury method, the samples are rendered hazardous to examine and thus no post-MICP examination of samples can be performed to determine what if any damage of samples occurred during the mercury intrusion that might bias results. It is the authors opinion that at the highest pressures, crushing of salt (including decrepitating of any fluid inclusions) and/or pore collapse probably occurs in some form, which would complicate interpretation of MICP results at those conditions.
5. The somewhat limited stroke of the odeometers used requires the use of spacers, and the hastelloy frits used here have the benefit of non-corrosiveness in the salt environment but have the drawback in that enough space or gaps exist between the

inner oedometer wall and the outer frit diameter. This was observed to permit salt creep into the gap and likely influenced the estimation of final porosity for Test 10. It may be possible to use Teflon heat-shrink roll covers to line the gap between the frit spacers and the oedometer walls.

6. There is no good correlation between mercury-determined porosities and sample porosities determined from geometrical considerations during salt consolidation. Largely this is because the MICP-determined porosity ignores pores larger than about 100 microns and is measured cumulatively from lower to the highest stresses. It is recommended that porosity determinations from helium methods (available in the Sandia Geomechanics Laboratory) be performed post-test in all salt consolidation experiments as a "sanity-check" on porosity determinations.

6. REFERENCES

Brantut, N., Baud, P., Heap, M.J., and Meredith, P.G., 2012, Micromechanics of brittle creep in rocks. J. Geophysical Research 117(B08412), doi:10.1029/2012JB009299.

Brantut, N., Heap, M.J., Meredith, P.G., and Baud, P., 2013, Time-dependent cracking and brittle creep in crustal rocks: A review, J. Structural Geology 52, 17-43.

Colombo, I., and Carli, F., 1981, Measurement of compressibility coefficient of nonporous polymer powders by mercury porosimetry: Powder Technology, v. 29, no. 2, p. 285-287.

Dewers, T. and Hajash, A., 1995, Rate laws for water-assisted compaction and stress-induced water-rock interaction in sandstones. J. Geophysical Research 100, 13093-13112.

Dullien, F. A. L., 1992, Porous media - fluid transport and pore structure, Second Edition: London, UK, Academic Press, Inc., 574 p.

Ko, T.Y. and Kemeny, J., 2011, Subcritical crack growth in rocks under shear loading. J. Geophysical Research, v. 116(B01407), doi:10.1029/2010JB000846.

Leverett, M.C., 1941, Capillary behavior in porous solids. Trans. AIME 142, 152-169.

Olson, R.K. and M.W. Grigg (2008) Mercury injection capillary pressure (MICP): A useful tool for improved understanding of porosity and matrix permeability distributions in shale reservoirs. Search And Discovery Article 40322.

Saadatpoor, E., Bryant, S., and Sepehrnoori, K., 2010, New trapping mechanism in carbon sequestration. Transport in Porous Media 82, 3-17.

Scholz, C., 1968, Mechanism of creep in brittle rock. J. Geophysical Research, v. 73, 3295-3302.

van Genuchten, R., 1978, Calculating the unsaturated hydraulic conductivity with a new closed-form analytical model. Water Resources Bulletin 78-WR-08, Department of Civil Engineering, Princeton University.

van Genuchten, R., 1980, A closed-form equation for predicting the hydraulic conductivity of unsaturated soils. Soil Science Society of America Journal 44, 892-898.

Washburn, E. W., 1921, The dynamics of capillary flow: Physical Review v. 17, p. 273-283

Webb, S., 2000, A simple extension of two-phase characteristic curves to include the dry region, Water Resources Research 36, 1425-1430.

Webb, S., 2006, Two-phase gas transport. In “Gas Transport in Porous Media” (Cliff Ho and Steve Webb, eds.), Springer, p. 55-70.

Appendix A: Technical Memo on First Phase of Testing

Sandia National Laboratories
Operated for the U.S. Department of Energy by
Sandia Corporation

Albuquerque, New Mexico 87185-

date: 5-15-2015

to: Christi Leigh, Cliff Howard, Kris Kuhlman

from: Thomas Dewers/06914

subject: Technical Memorandum: Lessons Learned From Preliminary Salt Testing

This Technical Memo summarizes 5 salt consolidation tests completed between May 7 and May 15, 2015 utilizing the new titanium oedometer system in 823/B-43A. These preliminary tests were run to facilitate preparation of a technical work document (TWD) for SNL Engineered Safety and to better define run conditions for future work. The resulting solid run products are shown in Figure 1.

Test 1 used Morton table salt from off-the-shelf; Tests 2-5 used WIPP Run-of-Mine (ROM) salt provided to Dewers by SNL Carlsbad Staff and with varying amounts of added water, compacted at 90oC and ~130 psi effective axial stress (axial stress minus pore fluid pressure). As anticipated, water is a critical component influencing creep consolidation; tests 3-5 were done with either saturated pores or 2% by weight added water for ~ 20 hours and resulted in tightly compacted relatively non-porous samples (Figures 1C-1E). Test 5 was run as a control at nominal room humidity at 90^{o}C for this same time period and was barely consolidated. Single "vugs" surrounded by tight relatively non-porous salt developed in the brine saturated tests and it is thought these tests developed an un-drained condition inadvertently sometime during the tests when expelled brine precipitated salt in the upper exit pore line due to cooling. Inside the oedometer vessel, pore fluid apparently migrated from collapsing pores to create a single "overpressured" brine-filled pore. By far the most successful test was Test 3, run with added 2% water but initially under-saturated pores. The results show that 1. Consolidated samples with substantially lessened porosity can be created overnight at 90^{o}C and low stresses using this apparatus; 2. Under-saturated pores but with added 2% brine produces tests with the most unequivocal results; and 3. Produced samples are suitable for testing for capillary pressure using mercury porosimmetry, and robust enough for transport.

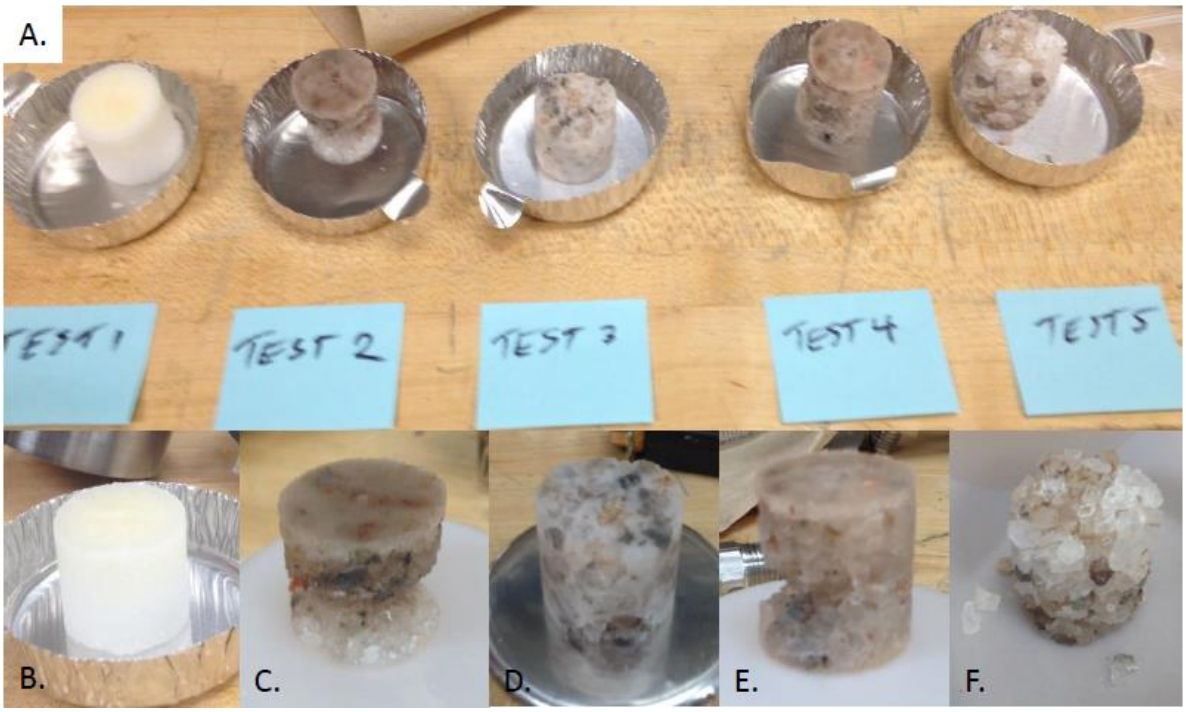

Figure 1. A. Salt cores from oedometric compression tests; B. Test 1; C. Test 2; D. Test 3; E. Test 4; F. Test 5.

A. Test Summaries

Test 1: This test used common table salt as a first run to demonstrate system capabilities, and to test the long-term stability of pressure and temperature control. The test was run over a ~5 day period and was run with a pore pressure using an initial solution of de-ionized water with added Morton salt to achieve a chemically saturated solution at salt room temperature solubility. Salt was loaded into the vessel with added water to excess (i.e. more water added to vessel+salt than needed to saturate the pore volume), pore pressure was increased to 339 psi to achieve a hydrostatic pressure condition; the vessel was heated to ~52^{o}C and held for an hour to check heating rates and temperature stability. Following this an effective stress of ~ 136 psi (680 psi axial stress minus 544 psi pore pressure) was established incrementally over a few minutes. These stress and pressure conditions were then held constant for approximately five days over the weekend. The result was a compacted and consolidated rock salt sample that is considered robust enough for mercury porosimetry testing (Figure 1B). A summary plot of Test 1 data is shown in Fig. 2. Dark blue curve is axial stress; light blue curve is pore pressure; green curve is axial displacement; red curve is sample chamber temperature, and orange curve is temperature of the ISCO pore pressure pump cylinder. The green curve shows the axial displacement and overall the creep portion of the curve is consistent with a compaction rate that decreases with the inverse of time (logarithmic creep).

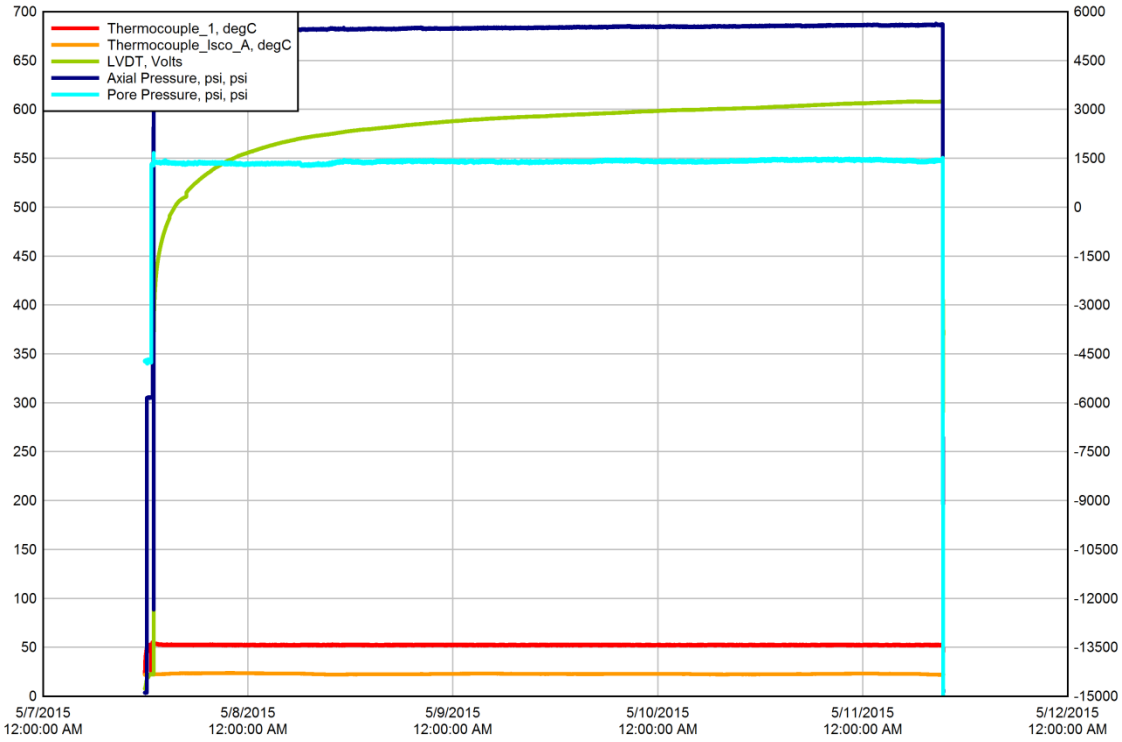

Figure 2. Temperature, pressure, axial stress, and axial displacement (LVDT) for Test 1 using Morton salt and brine-saturated pores. The left-hand y-axis is PSI for stress variables and degrees C for temperature. The right hand axis is in 10,000ths of an inch, so the test achieved compaction roughly equivalent to a 0.06th of an inch in axial displacement (roughly -3000 to 3000 in absolute displacement, starting when an effective axial stress was achieved and held constant).

Test 2: This test was the first in the series using WIPP ROM salt. Approximately 16 g of salt was loaded into the vessel with an excess of brine (distilled water chemically saturated with WIPP salt at room temperature). As determined by geometry of the oedometer and weight of salt (assuming a density of solid equivalent to halite of 2.17 g/cm3) that the starting porosity was about 48.3%. The test was run at 90^{o}C and 136 psi effective axial stress for ~ 18 hours. A summary plot of Test 2 data is shown in Fig. 3. Dark blue curve is axial stress; light blue curve is pore pressure; green curve is axial displacement; red curve is sample chamber temperature, and orange curve is temperature of the ISCO pore pressure pump cylinder. This was mostly a failed experiment as early into the test, the thermocouple connected to the temperature controller fell off the oedometer chamber and the temperature rose to ~120^{o}C. This resulted in a near step function increase in creep rate at this time. Another rapid increase in creep is seen at ~ 6:00 AM on 5/12/2015 with no apparent cause as seen in the unchanging stress, pressure, and temperature profiles. An interesting product of the run can be seen in Figure 1C, where a large "vug" is seen in the bottom third of the sample. When the test was ended, remaining brine was drained under gravity by opening the bleed valve connected to the bottom oedometer pore chamber. As a hypothesis, the vug may have developed under undrained conditions and the rapid increase observed in the latter part of the experiment could be explained by connection of previously undrained pores. This is discussed further with Test 4, where a similar vug was seen to develop.

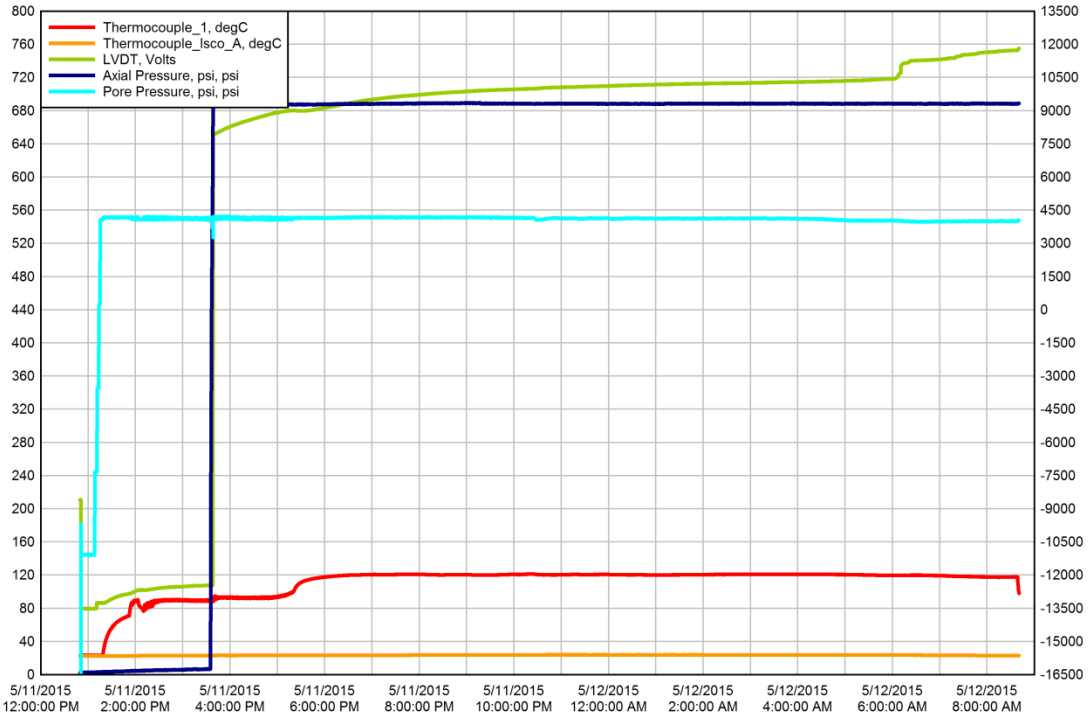

Figure 3. Temperature, pressure, axial stress, and axial displacement (LVDT) for Test 2 using WIPP ROM salt and brine saturated pores. The left-hand y-axis is PSI for stress variables and degrees C for temperature. The right hand axis is in 10,000ths of an inch, so the test achieved compaction roughly equivalent to a 0.04th of an inch in axial displacement (roughly +8000 to 12000 in absolute displacement, starting when an effective axial stress was achieved and held constant). The vessel temperature increased to 120^{o}C when the control thermocouple fell off the vessel at around 5:30 PM on 5/11/2015 resulting in a near step function increase in creep rate at this time. Another rapid increase in creep is seen at ~ 6:00 AM on 5/12/2015 with no apparent cause as seen in the unchanging stress, pressure, and temperature profiles.

Test 3: This test was run with WIPP ROM salt. Approximately 17 g of salt was loaded into the sample and ~0.3 chemically saturated brine was added (this represents about 2% of the total salt+brine weight). The salt was compacted over a period of about 20 hours at 90^{o}C and 136 psi effective axial stress. A summary plot of Test 3 data is shown in Fig. 4. The consolidation curve (shown in green) exhibits a smooth logarithmic relationship similar to that seen in Test 1. The light blue curve in Figure 4 shows a pore pressure that increases slightly with time for about ¾ of the total test time, presumably due to pore consolidation of air-filled pores under undrained conditions, near the vapor pressure of water at this temperature. The slight decrease seen near the end of the test may be due to a slight drop in room temperature barely observable in the orange curve (thermocouple attached to the ISCO pump cylinder.

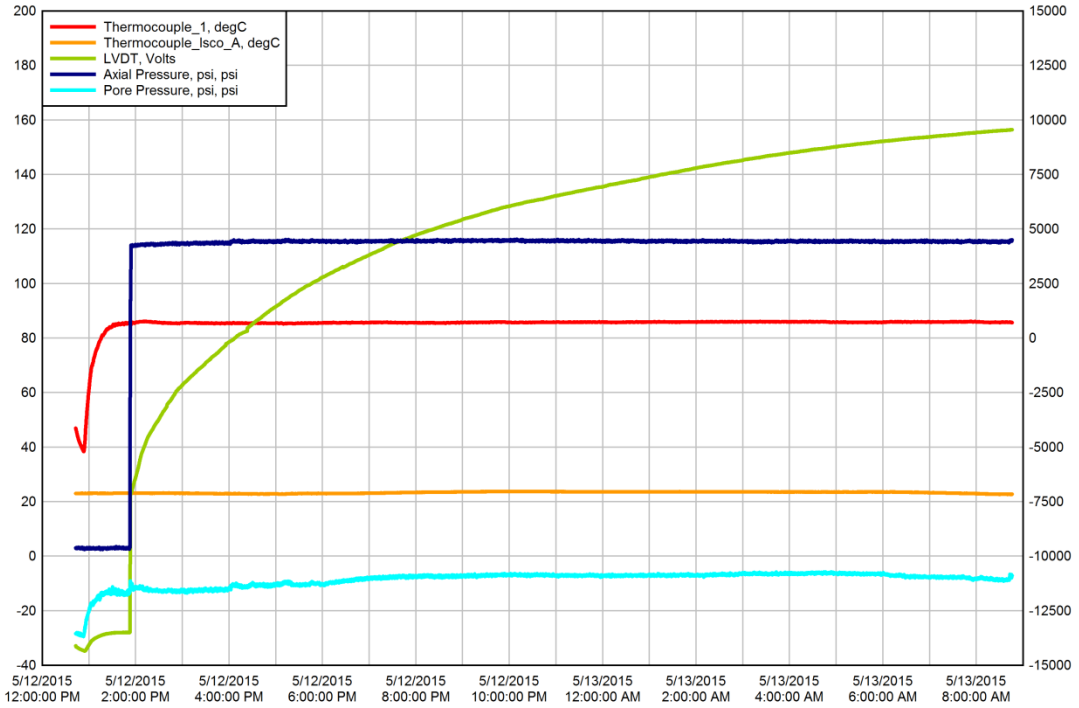

Figure 4. Temperature, pressure, axial stress, and axial displacement (LVDT) for Test 3 using WIPP ROM salt and added 2% by weight of brine. The left-hand y-axis is PSI for stress variables and degrees C for temperature. The right hand axis is in 10,000ths of an inch, so the test achieved compaction roughly equivalent to a 0.175^{th} of an inch in axial displacement (roughly -7500 to 10000 in absolute displacement, starting when an effective axial stress was achieved and held constant). This test achieved the most creep compaction in the series, and probably produced the most relevant results under drained conditions.

Test 4: This test was a repeat of Test 2 conditions measuring salt compaction with brine-saturated pores. Approximately 17 g of salt was loaded into the vessel with an excess of brine (distilled water chemically saturated with WIPP salt at room temperature). The salt was compacted over a period of about 21 hours at 90^{o}C and 136 psi effective axial stress. A summary plot of Test 4 data is shown in Fig. 5. Dark blue curve is axial stress; light blue curve is pore pressure; green curve is axial displacement; red curve is sample chamber temperature, and the orange curve is temperature of the ISCO pore pressure pump cylinder. Similar to Test 2, a large vug developed at some point during the run that did not drain by gravity at the end of the test, seen in Figure 1E. The exit port of the upper pore pressure line leading to the ISCO pore pump was seen post-test to be blocked by salt precipitation, and it is thought that this salt plugged the pore line from hot brine that was squeezed from the sample early in the test and precipitated salt upon cooling in the exit pore line. The sharp drop in creep rate at about 1 PM on 5/13/2015 could reflect a lowering of creep rate as the sample moved from undrained to drained conditions. The vug may have been a pocket of overpressured brine that developed under these undrained conditions.

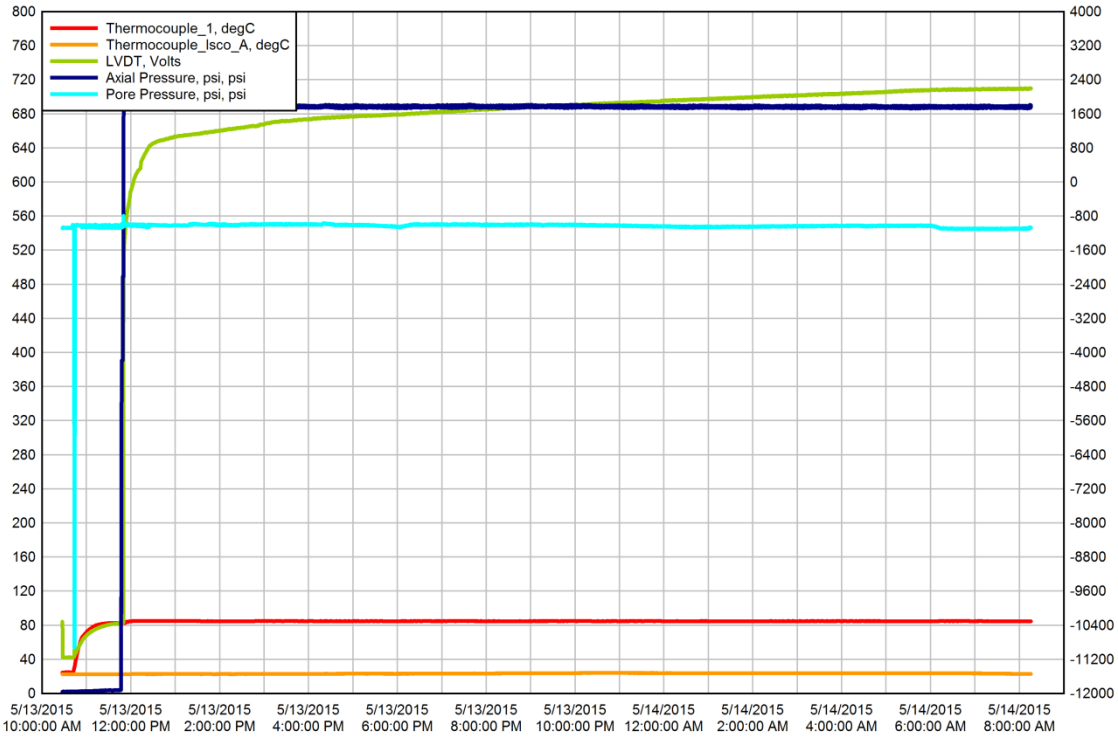

Figure 5. Temperature, pressure, axial stress, and axial displacement (LVDT) for Test 4 using WIPP ROM salt and brine-saturated pores. The left-hand y-axis is PSI for stress variables and degrees C for temperature. The right hand axis is in 10,000ths of an inch, so the test achieved compaction roughly equivalent to a 0.03th of an inch in axial displacement (roughly -800 to 2400 in absolute displacement, starting when an effective axial stress was achieved and held constant). The upper pore exit port was observed to have salt plugging it. A large "vug" of water was seen in the final solid run product (Figure 1C) which did not drain by gravity. The varying creep rate, vug, and observed salt plugging both suggest that the majority of the test was run under "undrained" conditions.

Test 5: This test was run using ~17g of WIPP ROM salt under nominal dry conditions and serves as a control test showing the influence of water on compaction rate when compared to the previous three tests. A summary plot of Test 5 data is shown in Fig. 6. Dark blue curve is axial stress; light blue curve is pore pressure; green curve is axial displacement; red curve is sample chamber temperature, and the orange curve is temperature of the ISCO pore pressure pump cylinder. This sample experienced the least amount of consolidation in this test series, and the resulting solid run product was friable and easily unconsolidated, as seen by the loose salt crystals in Figure 1F.

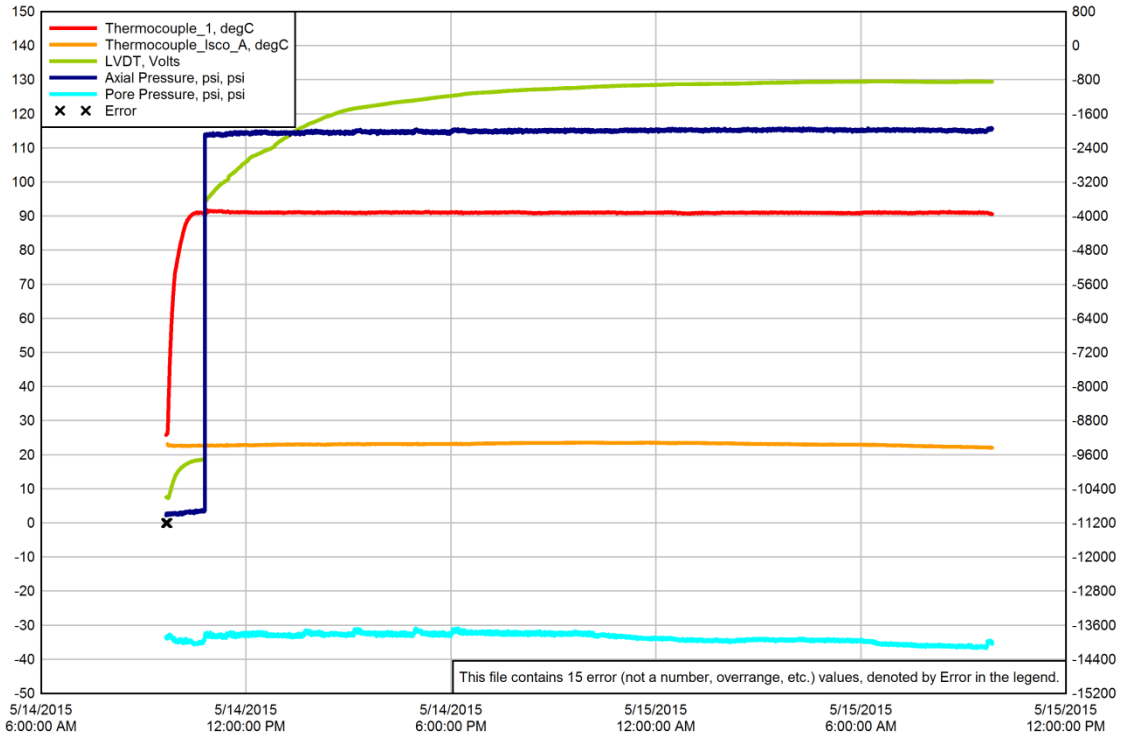

Figure 6. Temperature, pressure, axial stress, and axial displacement (LVDT) for Test 5 using WIPP ROM salt and no added water (nominal room humidity). The left-hand y-axis is PSI for stress variables and degrees C for temperature. The right hand axis is in 10,000ths of an inch, so the test achieved compaction roughly equivalent to a 0.027th of an inch in axial displacement (roughly -3500 to -800 in absolute displacement, starting when an effective axial stress was achieved and held constant). This is the least amount of creep compaction observed in the series and the resulting solid run product was barely consolidated (Figure 1F).

Comparison of Creep Rates

A comparison of the creep curves (green curves from the previous five figures) is shown in Figure 7. Test 3, with 2% added water (red curve), shows the greatest amount of compaction and the fastest rate, followed by the Test 1 Morton salt sample. It is possibly that the considerable amount of clay in the WIPP salt accelerated compaction of the relatively purer Morton food-grade salt. Test 4 (saturated with brine; purple curve) shows an early rate of compaction more or less equivalent to Test 3, but experiences a rapid drop in rate about one hour into the test that may coincide with clogging of exit pore lines by salt precipitation. Test 5, run nominally dry (orange curve) shows the least amount of overall consolidation. For Test 3, the initial porosity was found to be ~53%. The change in length of the sample from 0.504 in to 0.336 inches corresponds to a pore volume change from 0.209 in^3 to 0.073 in^3 or a drop in porosity to ~ 28.3% over about 20 hours.

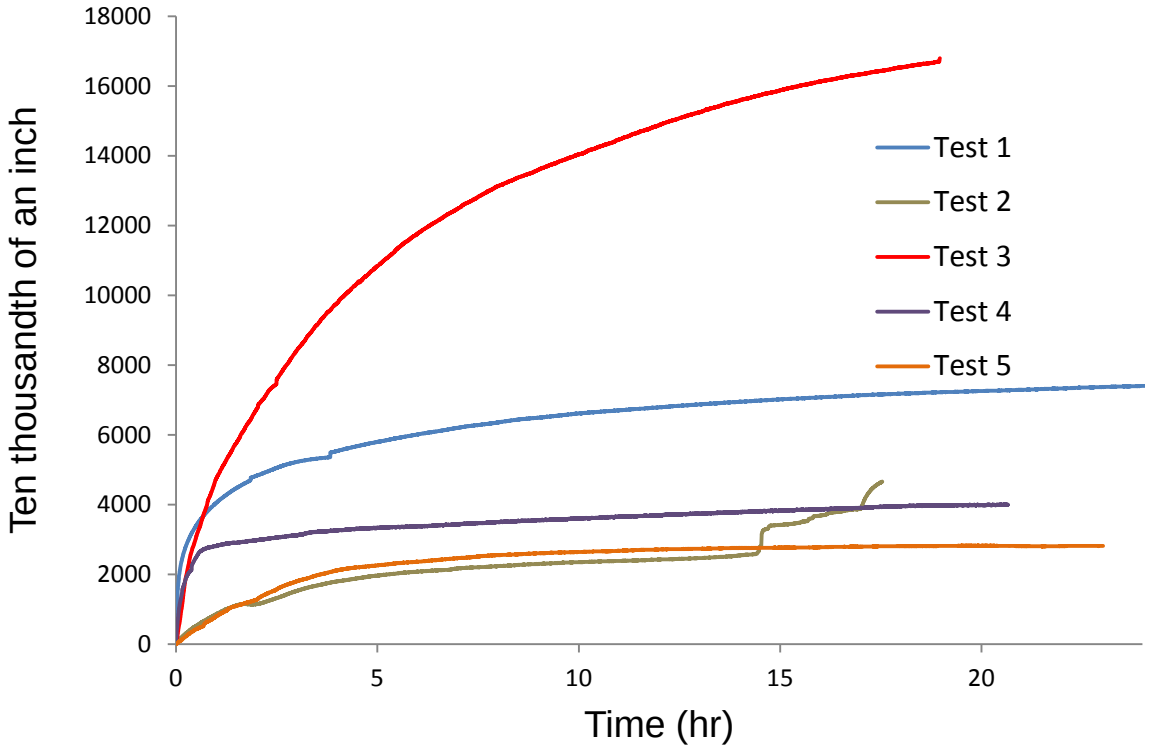

Figure 7. Comparison of creep curves, for ~20 hours, among the test series.

B. Conclusions and Lessons Learned

- This test series revealed a number of best-practices for conducting these types of tests using this apparatus, and these have been incorporated into a draft TWD and in particular the Operating Procedures contained within.
- Consolidation of WIPP ROM salt at 90°C with 2% added water compacts at a rate equivalent to brine-saturated pores under drained conditions.
- Compaction of brine saturated pores can result in an undrained or partially drained condition which could lead to equivocal conclusions. This was observed in both Test 2 and 4 using WIPP salt but was not the case observed with Test 1 using Morton salt. It appears that drained conditions can result with consolidation using saturated pores, but an undrained condition may be more difficult to achieve.
- There is a slight influence on pressure due to room temperature variations which could affect estimates of pore volume loss using the ISCO syringe volume change. However it appears that as the more accurate means of determining consolidation is using the LVDT and not pore volume expulsion measured by the ISCO, so this may not be important.
- Creep consolidation at 90°C with added water results in solid run products that should be viable for mercury porosimmetry tests.
- It would be interesting to compare capillary pressure curves of salt consolidated under a bulk undrained condition to that of a sample compacted to the same porosity but under drained conditions. The observation of formation of a single large vug in the samples compacted under presumed undrained conditions poses some interesting questions that could be investigated with this experimental protocol and apparatus.

Appendix B: Micromeritics Report on MICP

Distribution:

1	MS-0612	Review & Approval Desk, 9612. (electronic copy)
1	MS-0735	Moo Lee, 06914. (electronic copy)
1	MS-0747	Kristopher Kuhlman, 06224. (electronic copy)
1	MS-0751	Thomas Dewers, 06914. (electronic copy)
1	MS-1395	Christi Leigh, 06932. (electronic copy)
1	MS-1452	Cliff Howard, 02552. (electronic copy)
1	MS-0899	RIM-Reports Management, 9532. (electronic copy)


Sandia National Laboratories